Cell Reports

Article

# Structural basis of human cytomegalovirus neutralization by gB AD-5-specific potent antibodies

## Graphical abstract

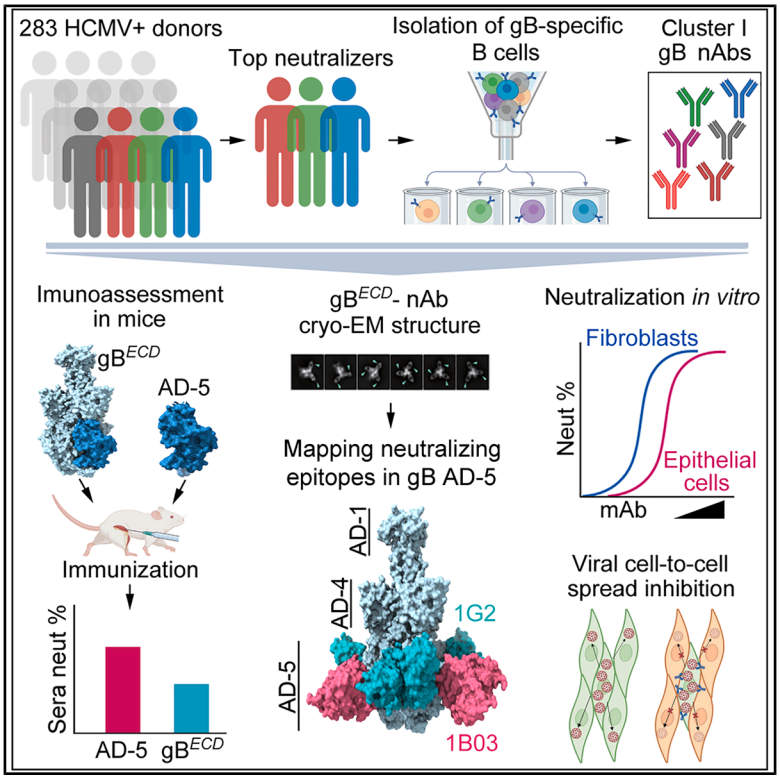


## Highlights

- Analysis of hCMV gB-specific memory B cells in top neutralizers yields cluster I nAbs
- Cluster I nAbs effectively inhibit viral cell-to-cell spread
- Cryo-EM structure reveals the mechanism of antibody neutralization
- Recombinant AD-5 induces superior nAb titers compared to $gB^{ECD}$ in mice


## Authors

Changwen Wu, Nan Song, Yizhen Zhao, ..., Zhiwei Yang, Shujia Zhu, Hua-Xin Liao

## Correspondence

wuchangwen@trinomab.com (C.W.), yzws-123@xjtu.edu.cn (Z.Y.), shujiazhu@ion.ac.cn (S.Z.), larryhliao@trinomab.com (H.-X.L.)



## In brief

Wu et al. identify potent cluster I nAbs that competitively target a unique epitope on hCMV gB AD-5, neutralize virus infection, and inhibit viral cell-to-cell spread. Structural analysis elucidates the hCMV neutralization mechanism. These data provide potential candidates for developing antibody-mediated therapy to effectively prevent and treat hCMV infection.


Wu et al., 2025, Cell Reports *44*, 115646
May 27, 2025 
https://doi.org/10.1016/j.celrep.2025.115646

CellPress

Cell Reports

CellPress
OPEN ACCESS

Article

# Structural basis of human cytomegalovirus neutralization by gB AD-5-specific potent antibodies

Changwen Wu,[1,7,*] Nan Song,[2,7] Yizhen Zhao,[3,7] Han Wang,[2] Yuanbao Ai,[1] Yayu Wang,[1] Yueming Wang,[1] Xiaohui Yuan,[1] Tong Liu,[1] Nan Li,[4,5] Dabbu Kumar Jaijyan,[6] Chengming Li,[1] Lei Zhang,[3] Weihong Zheng,[1] Zhiwei Yang,[3,*] Shujia Zhu,[2,*] and Hua-Xin Liao[1,8,*]

[1]Trinomab Pharmaceutical Co., Ltd., Zhuhai 519040, China
[2]Institute of Neuroscience, State Key Laboratory of Neuroscience, CAS Center for Excellence in Brain Science and Intelligence Technology, Chinese Academy of Sciences, Shanghai 200031, China
[3]MOE Key Laboratory for Nonequilibrium Synthesis and Modulation of Condensed Matter, School of Physics, Xi'an Jiaotong University, Xi'an 710049, China
[4]Department of Cell Biology, College of Life Science and Technology, Jinan University, Guangzhou 510632, China
[5]Guangdong Provincial Key Laboratory of Bioengineering Medicine, Guangzhou 510632, China
[6]Department of Microbiology and Molecular Genetics, New Jersey Medical School, Rutgers University, 225 Warren Street, Newark, NJ 070101, USA
[7]These authors contributed equally
[8]Lead contact
*Correspondence: wuchangwen@trinomab.com (C.W.), yzws-123@xjtu.edu.cn (Z.Y.), shujiazhu@ion.ac.cn (S.Z.), larryhliao@trinomab.com (H.-X.L.)
https://doi.org/10.1016/j.celrep.2025.115646

## SUMMARY

Human cytomegalovirus (hCMV) poses a severe threat to fetuses, newborns, and immunocompromised individuals. No approved vaccines and limited treatment options are current medical challenges. Here, we analyze the human B cell responses to glycoprotein B (gB) in three top hCMV neutralizers from a cohort of 283 individuals with latent-infected hCMV. By single-cell amplification of memory B cells, we identify a cluster of potent neutralizing monoclonal antibodies (nAbs) that competitively recognize an unknown vulnerable site on gB antigenic domain 5 (AD-5). This cluster of nAbs functionally outperforms the nAbs utilized in clinical trials. Cryoelectron microscopy (cryo-EM) unveils the structural basis of the neutralization mechanism of an antibody directly targeting the fusion subdomain on AD-5. Moreover, immunological analyses of human and mouse sera have preliminarily validated the potential superiority of AD-5-focused immune responses. Overall, our results will support the development of optimized gB-based vaccines and provide promising prophylactic and therapeutic antibody candidates against hCMV infection.

## INTRODUCTION

Human cytomegalovirus (hCMV) is ubiquitously distributed and establishes lifelong latency in humans. While hCMV infection is typically asymptomatic in healthy individuals, it can cause severe disease in fetuses, newborns, and immunocompromised patients.[1–4] Current treatment options, including CMV hyperimmunoglobulin (CMV-HIG) and antiviral drugs,[5–7] are limited by inadequate efficacy, side effects, and drug resistance.[8–10] Thus, developing effective vaccines and antibody therapeutics is crucial for preventing and treating hCMV infection.

Receptor binding and membrane fusion are essential for hCMV entry into cells, mediated by multiple envelope glycoproteins.[11] The heterotrimer gH/gL/gO interacts with platelet-derived growth factor receptor alpha (PDGFRα) to facilitate hCMV entry into various cell types,[12] while the pentamer gH/gL/UL128/UL130/UL131A binds to neuropilin-2 (Nrp2) to initiate viral internalization in epithelial cells.[13] The homotrimer glycoprotein B (gB) primarily functions as a fusogen, facilitating viral envelope fusion with cell membranes.[14,15] Consequently, gB is a promising vaccine target for inducing a broadly protective immune response. Notably, anti-gB immunoglobulin (Ig)Gs provide better protection against viral invasion in human trophoblast primary cells (TBPCs) compared to anti-pentamer IgGs.[16] Natural infection or vaccination with recombinant gB elicits robust immune responses and neutralizing monoclonal antibodies (nAbs).[17] The MF59-adjuvanted gB vaccine has shown 50% short-term protective efficacy from primary infection in seronegative postpartum women and significantly reduces viremia duration and antiviral treatment in solid organ transplant (SOT) recipients.[18,19] However, the protective effect of the gB/MF59 vaccine is believed to be primarily mediated by the non-neutralizing antibodies.[20,21] Therefore, these findings do not establish a clear correlation between vaccine efficacy and specific antibodies. Nevertheless, these

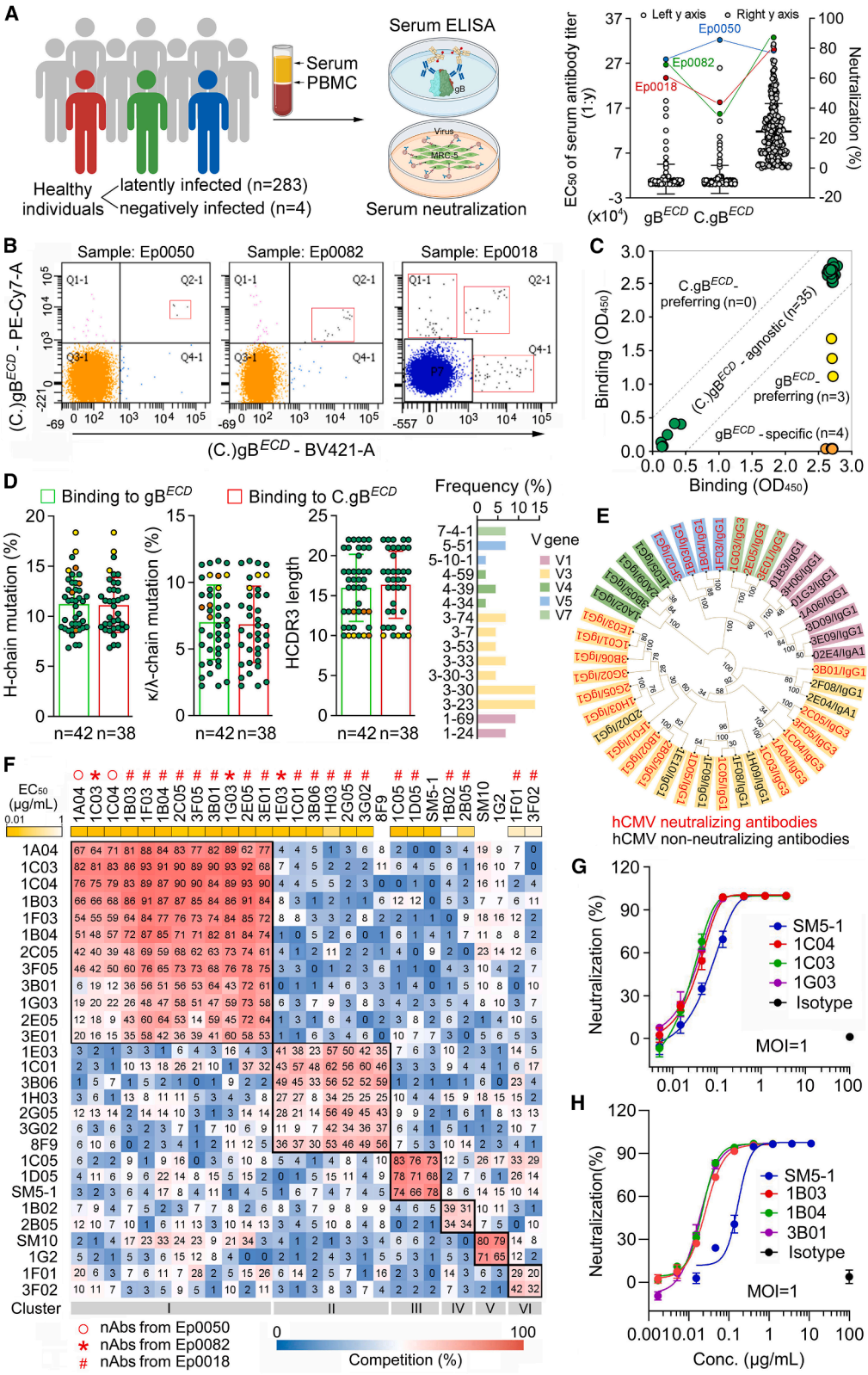


*(legend on next page)*

preliminary studies underscore the importance of hCMV gB as a vaccine target, while optimizing a gB-based vaccine is needed to elicit more durable and efficient immune responses.

Antibody immunotherapy against hCMV has the potential to address the limitations of current therapies and serve as an effective clinical alternative. hCMV gB-specific nAbs can inhibit the entry of cell-free virions and prevent viral cell-to-cell spread.[22–24] However, Novartis's CSJ148 did not achieve its primary endpoint despite showcasing antiviral activities in some recipients, such as reduced viral load, shorter median duration of preemptive therapy, and fewer courses of preemptive therapy.[25] Similarly, Roche's RG7667 also encountered setbacks in high-risk kidney transplant patients.[26] These setbacks might be partly due to the functional deficiencies in inhibiting viral cell-to-cell spread.[24,27] In contrast, antibodies are believed to reduce maternal transmission,[28] making prophylactic antibody application a promising strategy for CMV-negative, high-risk pregnant women. Additionally, studies suggest that HIG might enhance survival in SOT patients,[29,30] underlining the overall role of antibodies in hCMV prophylaxis and therapy.[29] The diverse routes of hCMV infection and transmission, along with their pathogenic stages, might be linked to the varied biological functions of antibody therapies,[31] particularly in inhibiting viral cell-to-cell spread. Therefore, developing more effective multifunctional antibody molecules should be a priority against hCMV infection.

Previous studies have revealed the conserved symmetric three-lobed architectures of the postfusion gB in herpes simplex virus (HSV), Epstein-Barr virus (EBV), and hCMV.[32–34] Despite these similarities, each gB possesses a unique domain arrangement, underscoring the importance of structural plasticity for virus-specific functions. In hCMV gB, six antigenic domains (AD-1 to -6) have been identified, with AD-4 and AD-5 being capable of inducing potent nAbs,[34–36] while AD-6 elicits non-neutralizing antibodies that impede viral cell-to-cell spread.[21] Notably, AD-5, an exposed domain, is targeted by nAbs and maintains similar local structures in both prefusion and postfusion gB.[37] However, the binding angle of SM5-1 to AD-4 in the prefusion structure requires adjustment to alleviate steric hindrance from domain III.[37] These studies provide a foundational framework for understanding the key immunogenic determinants in the gB protein.

In this study, we conducted a comprehensive analysis of the antibody response against gB in hCMV-seropositive individuals, identifying a panel of potent nAbs that competitively target previously uncharacterized antigenic determinants. Cryoelectron microscopy (cryo-EM) structural analysis revealed a unique mechanism of hCMV neutralization. Additionally, recombinant AD-5 demonstrated comparable immunogenicity and superior nAb titers compared to $gB^{ECD}$. These findings provide crucial insights for optimizing gB-based vaccines, particularly by focusing the immune response on AD-5 to elicit robust nAbs against these epitopes. Furthermore, the potent nAbs hold promise as candidates for the prevention and treatment of hCMV infection.

## RESULTS

### Individuals with latent-infected hCMV develop a potent nAb profile against the gB protein

To maximize the isolation of hCMV gB-reactive antibodies, we generated recombinant gB ectodomain proteins from both the widely used Towne strain ($gB^{ECD}$) and a highly homologous consensus gB ($C.gB^{ECD}$), derived from 61 available hCMV gB sequences in the NCBI database (Figure S1A). Three samples (Ep0050, Ep0082, and Ep0018) with high serum antibody titers against these antigens were selected and identified as top neutralizers (Figures 1A, S1B, and S1C). Fluorescence-labeled probes were used to sort hCMV gB antigen-specific memory B cells from these three top neutralizers (Figures 1B and S1D), yielding 42 monoclonal antibodies (mAbs) that are bound to $gB^{ECD}$. Of these, 35 mAbs also reacted with $C.gB^{ECD}$, while 3 mAbs showed a preference for $gB^{ECD}$, and 4 mAbs were specific to $gB^{ECD}$ (Figure 1C; Table S1). The mutation rates of the heavy- and light-chain variable (VH and VL) regions of these mAbs ranged from 8.13% to 16.57% and from 2.84% to 11.61% (Figure 1D; Table S1), respectively, indicating substantial somatic hypermutation. Sequence analysis revealed considerable variability in heavy-chain complementarity-determining region 3 (HCDR3) lengths and V gene distributions (Figure 1D). Twenty-four of 42 mAbs exhibited neutralization activity against the hCMV Towne strain in fibroblast cells (MRC-5) (Figure S2A), representing 14 distinct Ig gene clonal lineages (Table S1). A

**Figure 1. Isolation of potent nAbs against gB from individuals with latent-infected hCMV**

(A) Schematic diagram (left) and statistical analysis (right) of serum antibody titers and neutralizing activity in 287 healthy individuals. Data are represented as mean ± SD. The samples highlighted in colors were selected for subsequent analysis.

(B) Isolation of $gB^{ECD}$- and $C.gB^{ECD}$-specific memory B cells. Peripheral blood mononuclear cell (PBMC) samples were obtained from 3 individuals with latent-infected hCMV and sorted using FACS Aria III to isolate single memory B cells specific to $gB^{ECD}$ and $C.gB^{ECD}$. The sorted population is highlighted in red boxes. Due to the low frequency of double-positive memory B cells (binding both $gB^{ECD}$ and $C.gB^{ECD}$) in the Ep0050 and Ep0082 samples, both single- and double-positive B cells were collected from the Ep0018 sample.

(C) Apparent IgG-binding activity for $gB^{ECD}$ and $C.gB^{ECD}$ assessed by ELISA. Dashed lines indicate boundaries, with mAbs demonstrating a $\geq$1.5-fold difference in binding activity classified as preferential binders. All mAbs were tested at 0.1 μg/mL.

(D) Sequence annotation analysis including mutation frequencies of heavy chains and κ/λ light chains, amino acid lengths of heavy-chain CDR3, and usage frequency of heavy-chain V gene segments. Data are represented as mean ± SD.

(E) Phylogenetic tree generated for the heavy-chain V genes of 42 binding antibodies, arranged by V gene usage. nAbs are shown in red and non-neutralizing in black. The tree was constructed using MEGA 11.

(F) Cross-competitive binding assays were conducted for 24 isolated anti-gB nAbs and 4 reference nAbs (SM5-1, 8F9, 1G2, and SM10). Values in square boxes represent the percentages of cross-blocking. Hierarchical clustering based on the diagonal positive control identified six clusters. The neutralizing efficacy ($EC_{50}$) of each mAb *in vitro* is indicated on top. nAbs 1F01 and 3F02 (cluster VI) are undefined in this study.

(G and H) Neutralization activity of cluster I nAbs from 6 clonal lineages tested against the hCMV Towne strain in fibroblast cells. nAb SM5-1 served as a positive control, while an isotype antibody was used as a negative control. Data are represented as mean ± SEM from at least two independent experiments.

See also Figures S1–S3 and Table S1.

**A**

| Virus / mAb | Neutralization titers, $EC_{50}$ (μg/mL) | | | | |
|---|---|---|---|---|---|
| | Towne | TB40/E | BE/13/2012 | VR1814 | NR |
| 1C04 | 0.039 | 0.035 | 0.051 | n.d.* | n.d. |
| 1C03 | 0.026 | 0.015 | 0.055 | n.d. | n.d. |
| 1G03 | 0.036 | 0.027 | 0.027 | n.d. | n.d. |
| 1B03 | 0.025 | 0.091 | 0.006 | 0.156 | 0.159 |
| 1B04 | 0.022 | 0.028 | ≤0.006 | n.d. | n.d. |
| 3B01 | 0.018 | 0.025 | ≤0.006 | n.d. | n.d. |
| SM5-1 | 0.168 | 0.070 | 0.025 | n.d. | n.d. |

* Not done.

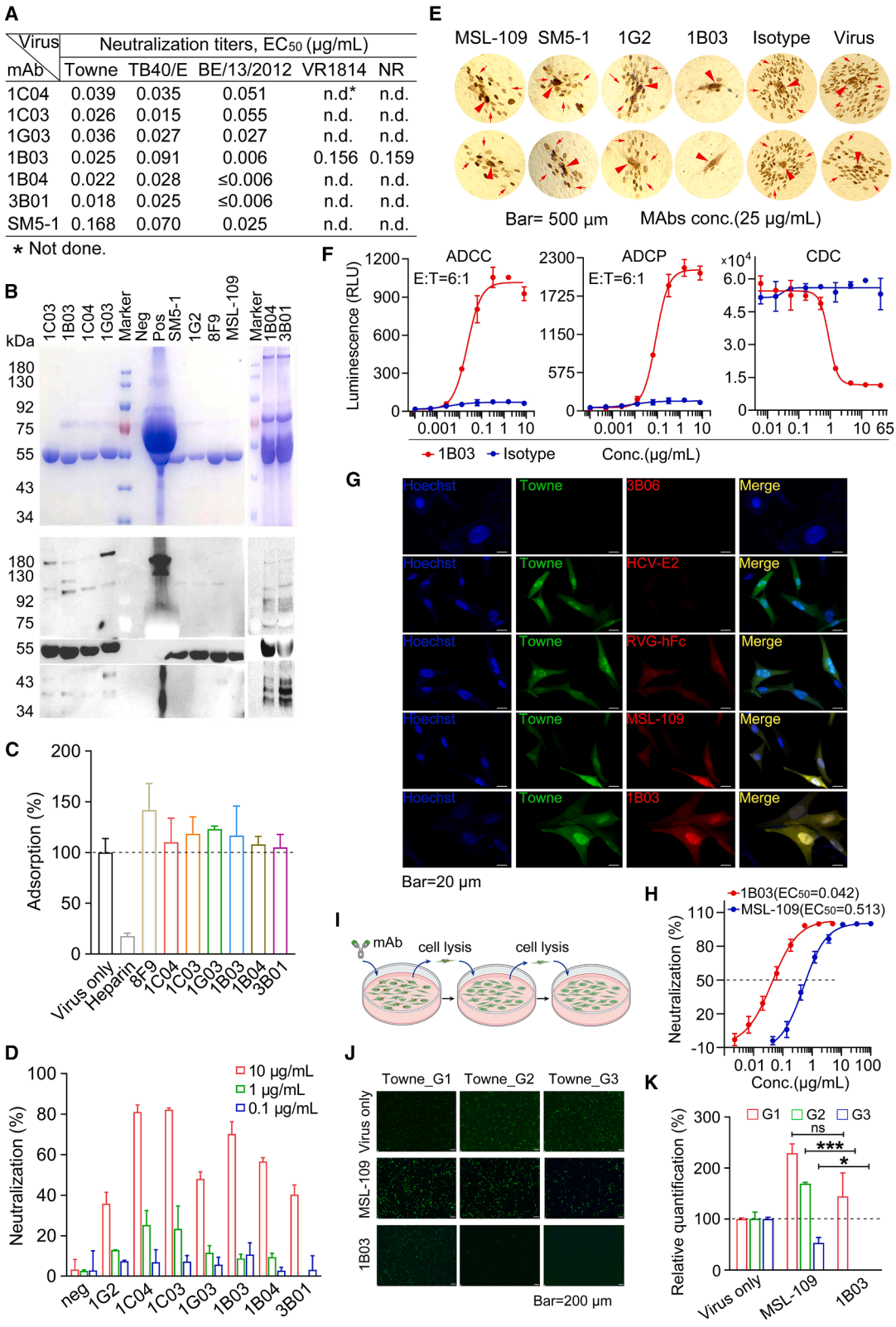


*(legend on next page)*

phylogenetic tree of 42 mAbs, based on their heavy-chain V gene sequences, classified them into five groups by variable gene usage (Figure 1E). V3, V5, and V7 genes were associated with nAbs, while mAbs from the V1 and V4 gene groups did not exhibit neutralizing activity, suggesting biased variable gene usage (Figure 1E).

Cross-competitive ELISAs classified the 24 nAbs into six clusters (Figure 1F). Three clusters of nAbs cross-competed with epitopes recognized by nAbs 8F9 (AD-2), SM5-1 (AD-4), or 1G2 and SM10 (AD-5) for binding to gB.[34,36,38] Epitope mapping through site-directed mutagenesis identified the epitopes targeted by AD-2-specific (cluster II) and AD-4-specific (cluster III) nAbs (Figures S3A and S3B). nAbs 1B02 and 2B05 (cluster IV) were found to recognize hCMV gB AD-1, as their binding depended significantly on disulfide bonds between Cys573 and Cys610 residues (data not shown). Cluster I nAbs derived from 7 different clonal lineages (Table S1) showed cross-blocking activity but did not block any reference nAbs (Figure 1F), indicating targeting of a potentially immunodominant site. Six potent nAbs (1C03, 1C04, 1G03, 1B03, 1B04, and 3B01) from cluster I, representing 6 clonal lineages, were selected for further characterization (Figures 1G and 1H; Table S1).

## Cluster I nAbs exhibit multiple antiviral functionalities

The six representative antibodies from cluster I exhibited comparable antiviral activity against various hCMV strains, with neutralization $EC_{50}$s ranging from 0.006 to 0.159 μg/mL (Figure 2A). Previous studies indicated that the clinical failure of mAb MSL-109 was partially attributed to its inability to bind to cell-free virions.[39,40] To evaluate the binding capabilities of cluster I nAbs, we conducted immunoprecipitation experiments, which revealed their ability to bind multiple virus-associated proteins, including gH or gH complexes (Figures 2B and S4A). This suggests that the epitopes recognized by cluster I nAbs are accessible on the viral surface. We also assessed whether cluster I nAbs could prevent hCMV binding to host cell surfaces. Unlike heparin-treated controls,[41] cluster I nAbs did not reduce the number of hCMV DNA copies at the cell surface (Figure 2C), indicating that they did not impede viral adsorption. Nonetheless, cluster I nAbs could neutralize hCMV after it had adsorbed onto cells, albeit at increased concentrations (Figure 2D). These findings imply that the antiviral activity of cluster I nAbs primarily occurs during the membrane fusion process following viral adsorption rather than at the initial adsorption stage.

Focusing on nAb 1B03 from cluster I nAbs, distinguished by high mutation rates in VH and VL (Table S1), robust neutralizing efficacy (Figure 2A), and strong binding affinity to gB (Figure S4B), we evaluated its ability to inhibit viral cell-to-cell spread. At concentrations of 25 μg/mL or greater, mAb 1B03 nearly completely blocked viral spread from initial replication centers to neighboring cells (Figure 2E) and outperformed reference nAbs MSL-109, SM5-1 and 1G2 (Figures 2E and S5A).[24] Other cluster I nAbs also effectively inhibited viral cell-to-cell spread (Figure S5B). Additionally, nAb 1B03 exhibited complement-dependent cytotoxicity (CDC), antibody-dependent cell cytotoxicity (ADCC), and antibody-dependent cell phagocytosis (ADCP) (Figures 2F, S6A, and S6B). Of note, nAb 1B03 does not bind autoantigens in HEp-2 epithelial cells (Figure S6C), indicating its lack of autoreactivity.

Previous studies have shown that hCMV infection induces the expression of viral Fc gamma receptors (vFcγRs).[42] Notably, we found that 1B03, along with MSL-109 and a control protein with human Ig Fc (RVG-hFc), penetrated the hCMV-infected cells but not the uninfected cells (Figure 2G). This suggests that the entry of antibodies into infected cells might be facilitated by vFcγRs, such as human-like FcγRI (Figure S6D). To determine the effect of intracellular antibodies on hCMV growth, we introduced mAbs into hCMV-infected cultures and passaged the viruses for three rounds (Figure 2I). Given their equivalent neutralizing potencies (Figure 2H), we added MSL-109 (100 μg/mL) and 1B03

**Figure 2. Identification of the biological functions of antibodies**

(A) Neutralization activity of cluster I nAbs against multiple hCMV strains. The effective concentration required to infect 50% of cells ($EC_{50}$) was determined based on relative fluorescence intensity for the Towne and TB40/E strains in human fetal lung fibroblasts (MRC-5) and by specific cytopathic plaque for clinical isolate BE13/2012 on MRC-5 and IE1/IE2 expression for the VR1814 and NR strains on human retinal pigment epithelial cells (ARPE-19).

(B) Immunoprecipitation of hCMV virions with cluster I nAbs and reference nAbs. Samples were analyzed via SDS-PAGE (top) and immunoblotting with hCMV-positive serum to detect virus-associated proteins (bottom). "Neg" indicates virus incubation with protein A beads without antibody, while "pos" indicates the concentrated virus suspension used in the immunoprecipitation.

(C) Effect of cluster I nAbs on hCMV virions adsorption to host cells. The amounts of hCMV virions adsorbed to the cell surface were quantified by qPCR. Heparin (10 μg/mL), known to block virus adsorption, served as a positive control. Data are represented as mean ± SEM.

(D) Neutralization of cell-surface-adsorbed hCMV virus by cluster I nAbs. Neutralization percentages were measured by relative fluorescence intensity compared to virus control. Data are represented as mean ± SEM.

(E) Inhibition of viral cell-to-cell spread in fibroblast cells. hCMV-infected cells (brown dots) were detected by immunohistochemistry using anti-IE1/IE2 antibody. Smaller brown dots (indicated by arrows) represent IE1/IE2-positive cells as satellite viral infection foci, while larger, darker brown dots (indicated by red arrowheads) are shown as initial replication centers.

(F) Antibody-mediated cytotoxicity (CDC and ADCC) and phagocytosis (ADCP) to gB-stabilized Chinese hamster ovary (CHO) cells (target [T]) by guinea pig serum and effector cells (Jurkat-FcγRIIIa V158 and Jurkat-FcγRIIa H131) (effector [E]). Data are represented as mean ± SEM.

(G) Intracellular entry of antibodies in hCMV-infected cells. Cell nuclei are shown in blue, green fluorescence indicates viral infection signals, and red fluorescence represents the antibodies or proteins entered into the cells.

(H) Neutralization activity of 1B03 and MSL-109 against the Towne strain in MRC-5 cells. Data are represented as mean ± SEM.

(I) Schematic representation of consecutive passages of lysates from hCMV-infected cells with antibody addition post-infection.

(J) Consecutive passages of Towne strain with MSL-109 (100 μg/mL) and 1B03 (10 μg/mL). The intensity of green fluorescence reflects the level of viral infection.

(K) Relative viral titers for each generation measured by fluorescent qPCR. Data are represented as mean ± SEM. Statistical analysis was performed using a two-tailed unpaired t test (*$p < 0.05$ and ***$p < 0.001$).

See also Figures S4–S6.

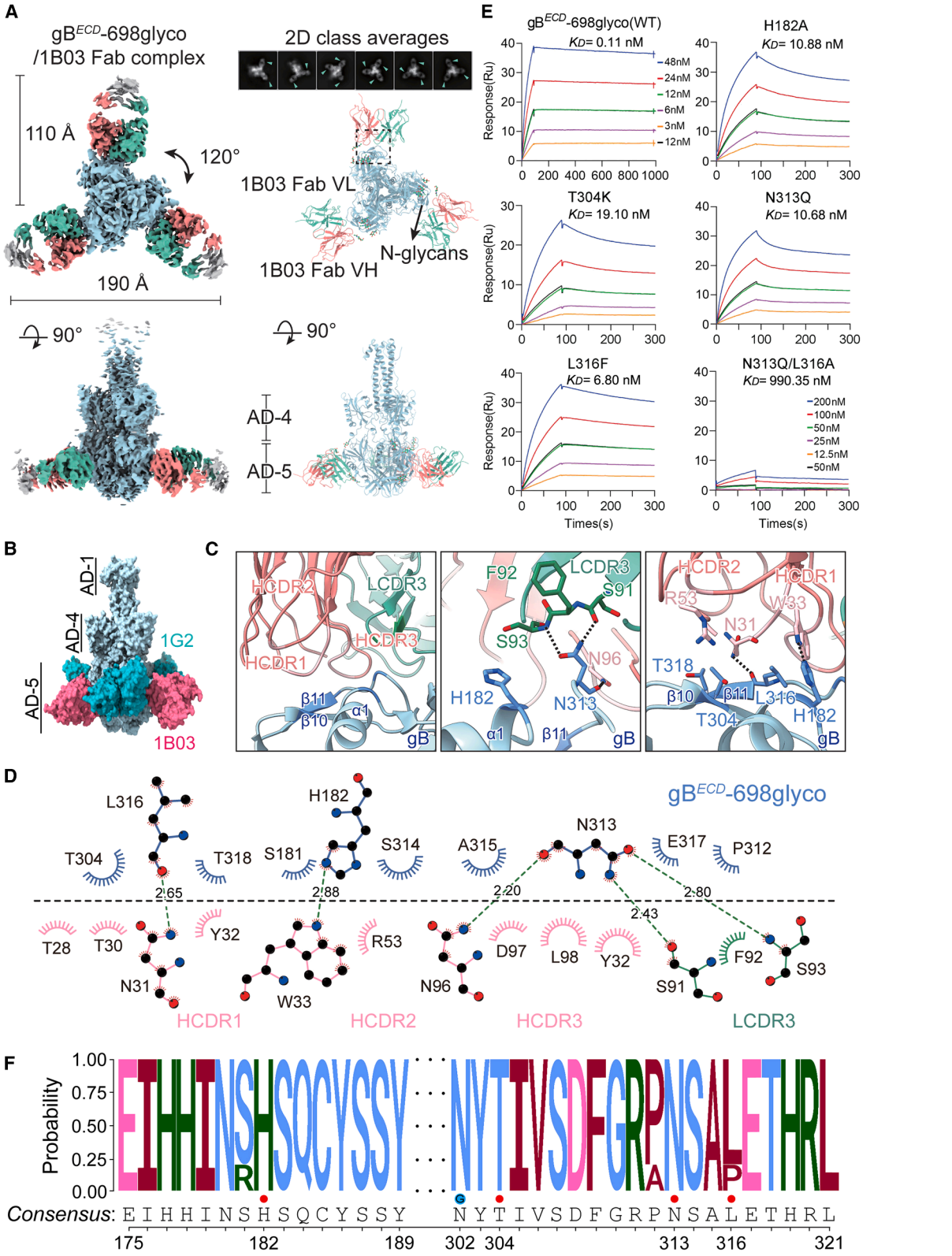


*(legend on next page)*

(10 μg/mL) after hCMV inoculation. The re-infection of fresh cells with lysates from first-generation CMV-infected cells (Towne-G1) showed that 1B03 significantly reduced the number of infected cells in the second round (Towne-G2) and nearly eliminated the infected cells in the third round (Towne-G3) (Figures 2J and 2K). In contrast, MSL-109 had a minimal impact on virus growth during the second and third rounds (Figures 2J and 2K). These results indicate that 1B03 effectively inhibits subsequent rounds of hCMV infection, suggesting that the intracellular 1B03-like antibodies might reduce viral growth in latently infected cells *in vivo* and potentially influence hCMV transmission in tissues. However, the precise mechanism by which 1B03 inhibits virus growth in cells remains to be elucidated.

## Cryo-EM structure reveals molecular basis of gB/1B03 interface

Cryo-EM analysis was performed to elucidate the atomic structure of the hCMV gB protein complexed with mAb 1B03. The complex was generated by incubating purified $gB^{ECD}$-698glyco with 1B03 Fab at a molar ratio of 1:3, as confirmed by fluorescence-detection size-exclusion chromatography (FSEC). The FSEC profiles displayed a shift in the absorbance peak, indicating the formation of a higher-molecular-weight gB-1B03 complex compared to the individual components (Figures S7A and S7B). Single-particle cryo-EM was subsequently utilized to determine the interaction mode between 1B03 Fab and hCMV gB, yielding a 3.0 Å resolution structure of the gB/1B03 Fab complex (Figure S7C; Table S2). High-quality density maps of the complex facilitated the construction of an accurate atomic model, including side-chain orientations and N-glycosylation modifications (Figures S7D, S7E, and S8). The complex exhibited a clover-like arrangement, with the gB trimer at the center and the three 1B03 Fabs tethered as leaflets (Figure 3A). We identified a unique antigenic determinant on AD-5 (Figure 3B) that differed from previously reported epitopes.[36] Notably, all three HCDRs and the light-chain CDR3 (LCDR3) involved direct contact with gB. Specifically, helix α1, strand β10, and β11 contributed significantly to the gB/1B03 Fab interaction (Figures 3C and S7F). Hydrogen bonds were observed between the backbones of Leu316, Thr318, and Thr304 and the side chain of His182 in gB AD-5 with Asn31 and Trp33 in HCDR1 (Figure 3D). Additionally, hydrophobic interactions were noted in the side chains of Leu316 and Thr304 in gB AD-5 contacts with Trp33 in HCDR1 and Arg53 in HCDR2, respectively (Figure 3D). Asn313 in gB AD-5 formed hydrogen bonds with the side chain of Ser91 and the backbone atoms of Ser93 in LCDR3, as well as Asn96 in HCDR3 (Figures 3C and 3D). Overall, 1B03 mainly utilizes its HCDRs to interact directly with AD-5.

To validate these structural insights, alanine substitution and polar switch mutations were introduced at gB residues involved in the binding interface identified by cryo-EM. Binding affinity to 1B03 was measured using surface plasmon resonance (SPR). The His182Ala mutation resulted in a nearly 100-fold decrease in binding affinity (Figure 3E; Table S3), while mutations at position 318 (Thr318Lys), 316 (Leu316Phe), 313 (Asn313Gln), or 304 (Thr304Lys) led to a 17- to 173-fold decrease in binding affinity (Table S3). Additionally, the dual mutation Asn313Gln/Leu316Ala virtually abolished the binding of gB to 1B03, which was the most significant compared to other combined mutations (Table S3), highlighting the synergistic roles of Asn313 and Leu316 in maintaining the conformational integrity of the gB/1B03 interface. Sequence alignment of gB fragments from the tested hCMV strains revealed the high conservation of amino acid residues within the 1B03 epitope (Figure 3F), with the only variation at Leu316, which directly interacts with 1B03 (Figures 3D and 3F).

## Key residues Asn313 and Leu316 in the β10-loop-β11 structure form the shared backbone of epitopes for cluster I nAbs

Despite variability in Ig gene families and the lengths of HCDR3, LCDR1, and LCDR3 (Figure 4A), class I nAbs exhibited comparable affinity and neutralizing activity (Figures 2A and S4B). The binding of class I nAbs to the gB protein could completely block each other (Figure 1F), suggesting shared characteristics among their epitopes. The indistinguishable binding of cluster I nAbs to both $gB^{ECD}$ and AD-5 supports the use of AD-5 for studying the epitope characteristics of these nAbs (Figure 4B).

To explore this, we constructed models of the epitopes for nAbs 1B03, 1B04, 1C03, 1C04, 1G03, and 3B01 interacting with AD-5, utilizing the cryo-EM structure of the gB/1B03 complex as a template (Figures 4C–4H, S9A, and S9B) via the MODELER program.[43] The modeling indicated that Leu316 on the β11 sheet and/or Asn313 in the adjacent loop of gB formed hydrophobic interactions or hydrogen bonds with specific residues in cluster I nAbs, respectively (Figure S9C). Notably, dual mutations Asn313Gln/Leu316Ala in the gB protein reduced the affinity of cluster I nAbs, with the mutation completely abolishing

**Figure 3. Structure insight and binding mechanism of gB/1B03 Fab complex**

(A) Cryo-EM density (left) and atomic model (right) of $gB^{ECD}$-698glyco/1B03 Fab complex, viewed from down-top (top) and side view (bottom). Inserted on the top are representative two-dimensional (2D) class averages of the complex with 1B03 Fab indicated by green triangles. The glycans on specific Asn residues at positions 208, 281, and 302 are observed and displayed in atomic mode.

(B) Model of nAbs 1G2 and 1B03 simultaneously bound to AD-5.

(C) Binding interface between $gB^{ECD}$-698glyco and 1B03 Fab. The $gB^{ECD}$-698glyco, heavy chain, and light chain of 1B03 Fab are depicted in light blue, light coral, and aquamarine, respectively. Key binding residues are highlighted and shown in sticks. Complementarity-determining regions (CDRs) of the heavy and light chains are abbreviated as HCDRs or LCDRs, respectively.

(D) Schematic diagram of the $gB^{ECD}$-698glyco/1B03 Fab interface was plotted using Ligplot$^{+}$. Hydrogen bonds are represented by dashed lines, and hydrophobic interactions are depicted by arcs with spokes.

(E) Affinity for 1B03 binding to $gB^{ECD}$-698glyco and its mutants. The association and dissociation curves were measured using SPR.

(F) Sequence conservation of the 1B03 epitope peptides across hCMV strains in Figure 2A was analyzed using Sequence LOGO Map (https://www.omicshare.com/tools/Home/Soft/seqlogo). Key residues involved in direct contact with 1B03 Fab are marked with red dots.

See also Figures S7, S8, and S10 and Tables S2 and S3.

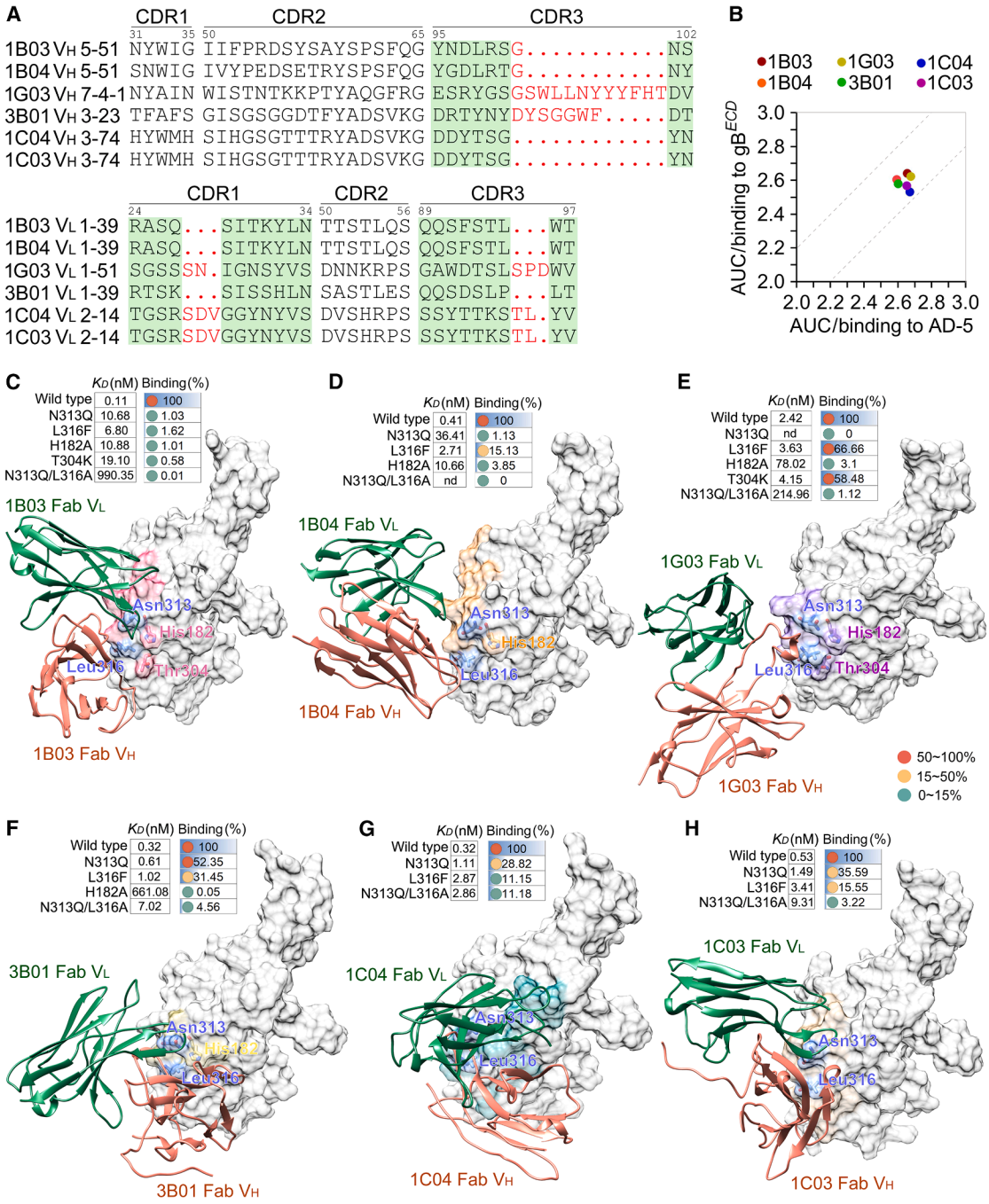


**Figure 4. Binding profiles of gB AD-5 with cluster I nAbs**

(A) Sequence alignment of H/LCDRs of cluster I nAbs.

(B) Comparison of the binding activity, expressed as area under curve (AUC), of cluster I nAbs to AD-5 (in *x* axis) and $gB^{ECD}$ (in *y* axis). The dashed lines serve as boundaries for showing variations in binding activity of antibodies to these 2 proteins. All 6 data points were clustered together within the dashed lines.

(C–H) Surface representation of hCMV gB AD-5 with neutralizing epitopes of mAb 1B03 (C), mAb 1B04 (D), mAb 1C03 (E), mAb 1C04 (F), mAb 1G03 (G), and mAb 3B01 (H) by MODELER program. Residues Asn313 and Leu316 are uniformly shown in a medium blue atomic model, while epitope-specific residues are indicated by their respective colors. Binding activities of each of 6 cluster I nAbs to gB mutant proteins with single or dual residual substitution are indicated on the top of each modeled pattern diagram. "nd" indicates no binding detected.

See also Figure S9 and Table S3.

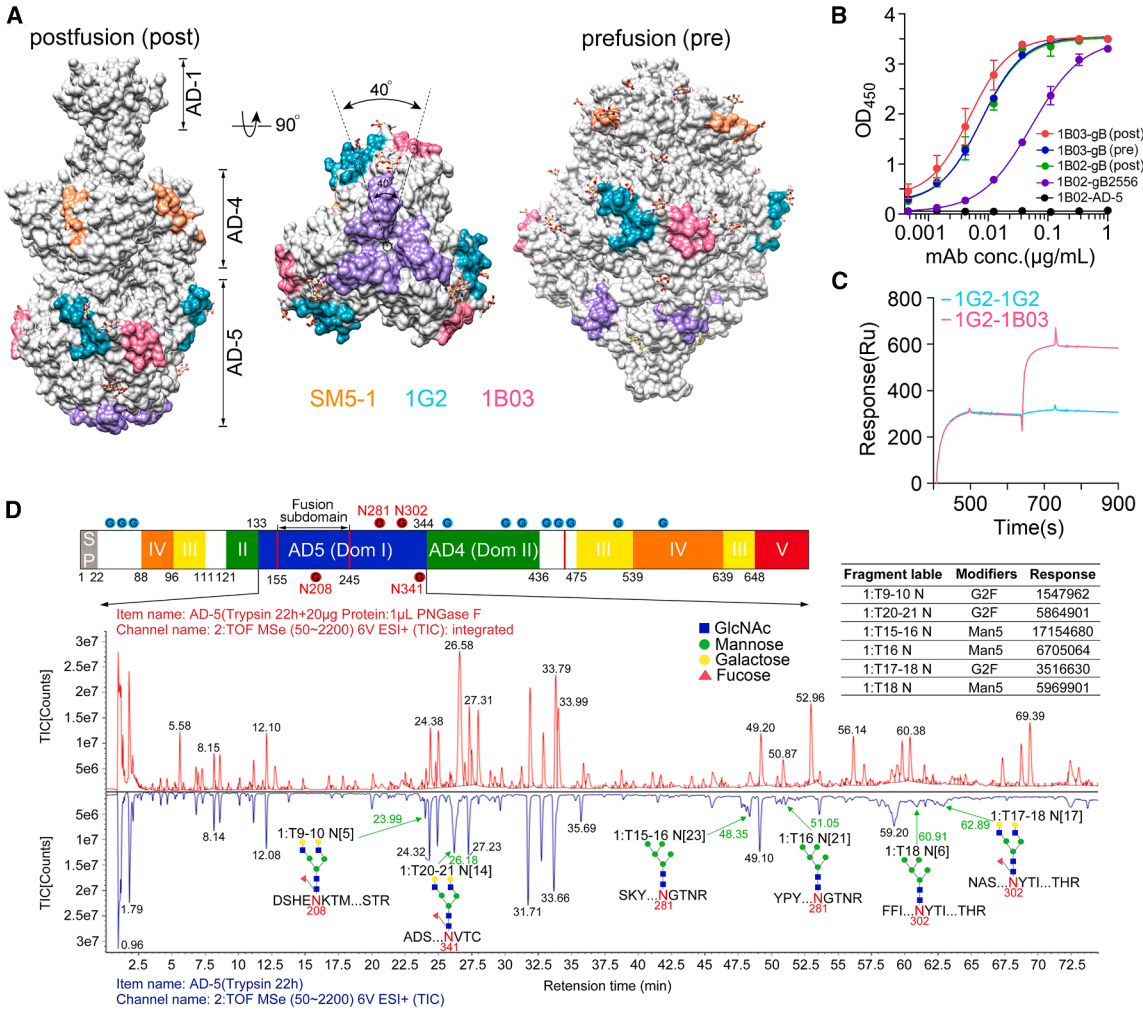


*(legend on next page)*

the binding of 1B04 (Figures 4C–4H; Table S3). These results highlight the critical role of the β10-loop-β11 structure, where Asn313 and Leu316 reside, in sustaining the high affinity of cluster I nAbs to gB.

Cluster I nAbs also exhibited distinct molecular interaction profiles. His182 in gB formed a strong hydrophobic interaction with the side chain of Trp100C in HCDR3 of 1G03 (Figure S9C; Table S3) and is essential for binding by 1B03, 1B04 and 3B01 (Figures 4C, 4D, and 4F; Table S3). Additionally, Thr304 significantly facilitated the binding of 1B03 to gB (Figure 4C; Table S3). However, mutations in His182 and Thr304 did not significantly affect the binding of 1C04 and 1C03 to gB (Table S3).

## Newly identified epitope is spatially independent and well exposed without glycosylation

The epitope on AD-5 targeted by the hCMV gB nAb 1G2 is defined by residues Tyr280-Phe300.[36] Notably, while the key segment (Thr304-Thr318) of the 1B03 epitope is adjacent to the 1G2 epitope in the primary structure, these two epitopes are independent, exhibiting a mirror-symmetric distribution on AD-5 with an approximate spatial angle of 40° (Figure 5A). This distribution is also evident in the prefusion gB (Figures 5A and 5B), as AD-5 maintains a consistent local structure in both forms.[37] SPR assays confirmed the independence of these epitopes, showing no competition between 1G2 and 1B03 (Figure 5C).

In contrast to HSV-1 and EBV, the hCMV gB is extensively shielded by a dense layer of glycans.[34] Cyro-EM structure analysis of AD-5 identified multiple N-glycosylation sites (Figure 3A). To explore the glycosylation details, we performed glycopeptide analysis for AD-5 using ultra-performance liquid chromatography-tandem quadrupole-TOF (Q-TOF) mass spectrometry (UPLC-MS/MS). De-N-glycosylation analysis, where various glycosylation sites were converted from Asn to Asp using NGase F, revealed four occupied N-glycosylation sites (Figure 5D), none located within the 1B03 epitope segment. Asn281 and Asn302 were predominantly occupied by high-mannose-type glycan Man5GlcNAc2 (Man5) (Figure 5D), whereas Asn208 and Asn341 were primarily occupied by heterogeneous glycan structure G2F GlcNAc2 (G2F) (Figure 5D). Asn313 showed no N-glycan modification.

To assess the influence of N-glycans on 1B03 binding, recombinant $gB^{ECD}$ was treated with an increasing dosage of PNGase F to remove N-linked glycans. The molecular mass of gB monomers decreased progressively with increasing dosage of PNGase F (Figure 5E). 1B03 exhibited strong binding to progressively deglycosylated monomers and trimers (Figure 5E). Moreover, SPR analysis demonstrated that 1B03 maintained comparable affinity to $gB^{ECD}$ before and after treatment with PNGase F (500 U/μg) (Figure 5F). Furthermore, O-glycosylation sites on $gB^{ECD}$ were prevalent in certain regions (residues 1–100 and 400–500) but absent in the vicinity of the epitope identified in this study (Figure 5G). Together, these findings suggest that the newly identified epitope is unique and sufficiently exposed and that the binding of 1B03 to it is independent of the N/O-glycosylation state of gB.

## Natural infection and passive immunization highlight the potential superiority of AD-5-focused immune responses against hCMV

Different ADs on hCMV gB exhibit varying reactivity with human serum antibodies.[44] We analyzed 287 human serum samples for their reactivity to both AD-5 and $gB^{ECD}$. Approximately 98% of serum samples were reactive to $gB^{ECD}$, while under 13% showed moderate reactivity to AD-5, with less than 5% demonstrating strong reactivity to AD-5 (Figures 6A and 6B). Correlating antibody titers from AD-5 and $gB^{ECD}$ with heat-inactivated serum neutralization assays revealed a moderate correlation for AD-5-reactive antibody titers (Pearson's $r^2$ = 0.481) (Figure 6C), whereas $gB^{ECD}$-reactive antibody titers correlated poorly with serum neutralization (Figure 6D). In healthy individuals, serum samples with high AD-5-reactive antibody titers ($OD_{450}$ > 1.0 at 1:1,000 dilution; $n$ = 49) exhibited significantly superior neutralizing activity compared to those with low AD-5-reactive antibody titers ($OD_{450}$ < 1.0 at 1:1,000 dilution; $n$ = 238) (Figure 6E). Notably, 43% of individuals with high AD-5-reactive antibody titers exhibited strong neutralizing potency (>50%) (Figure 6F). As anticipated, serum neutralization was greatly reduced in AD-5 antibody-depleted samples (Figure 6G), emphasizing the critical role of AD-5-reactive antibodies in antiviral activity.

Two potent neutralizing epitopes have been identified on AD-5, making it an attractive candidate for vaccine development. We

**Figure 5. Distribution mode and characteristics of the newly identified epitope**

(A) Surface representation of gB in both postfusion (PDB: 7YRN) and prefusion (PDB: 7KDP) conformations, highlighting neutralizing epitopes. The epitopes include residues Tyr280-Phe300 (1G2, cyan), Ser181-Ser183 and Thr304-Thr318 (1B03, salmon), and Glu359-Asp362 and Lys379-Asn383 (SM5-1, orange). Fusion loop peptides are shown in light purple, and simple glycans modeled into glycosylation sites are represented as colorful sticks.

(B) Binding of 1B03 to the prefusion (pre) and postfusion (post) gB proteins. The gB (pre) was designed and expressed in Expi293F cells.[37] Data are represented as mean ± SEM. 1B02 serves as a validating antibody targeting hCMV gB AD-1, which shows different molecular arrangement and exposure in both pre- and postfusion gB protein.[37]

(C) Non-competitive epitope binding of 1G2 and 1B03 to hCMV gB protein was evaluated using SPR.

(D) N-glycosylation analysis of hCMV gB AD-5 by UPLC-MS/MS. Site-specific core glycan structures on AD-5 were confirmed with high confidence by comparing the ion flow diagrams of N-glycosylated peptides before (blue) and after (red) treatment with PNGase. Four identified N-glycosylation sites are marked with red circles, while the other predicted sites are indicated with blue circles in the schematic of $gB^{ECD}$.

(E) Deglycosylation of $gB^{ECD}$ with PNGase F, with quantities indicated at the top of the gels, followed by separation in 10% SDS-PAGE. A control sample of $gB^{ECD}$ was completely deglycosylated under denaturing condition (*). Gels were stained with Coomassie blue (top) or immunoblotted with 1B03 under native condition (bottom).

(F) Binding kinetics of 1B03 to $gB^{ECD}$ and deglycosylated $gB^{ECD}$ were measured using SPR.

(G) Analysis of O-GalNAc glycosylation sites in gB protein (residues 1–698) using NetOGlyc-4.0 software. Residues Ser (S) or Thr (T) with scores above the threshold (0.5) were defined as O-GalNAc glycosylation sites.

See also Tables S4 and S5.

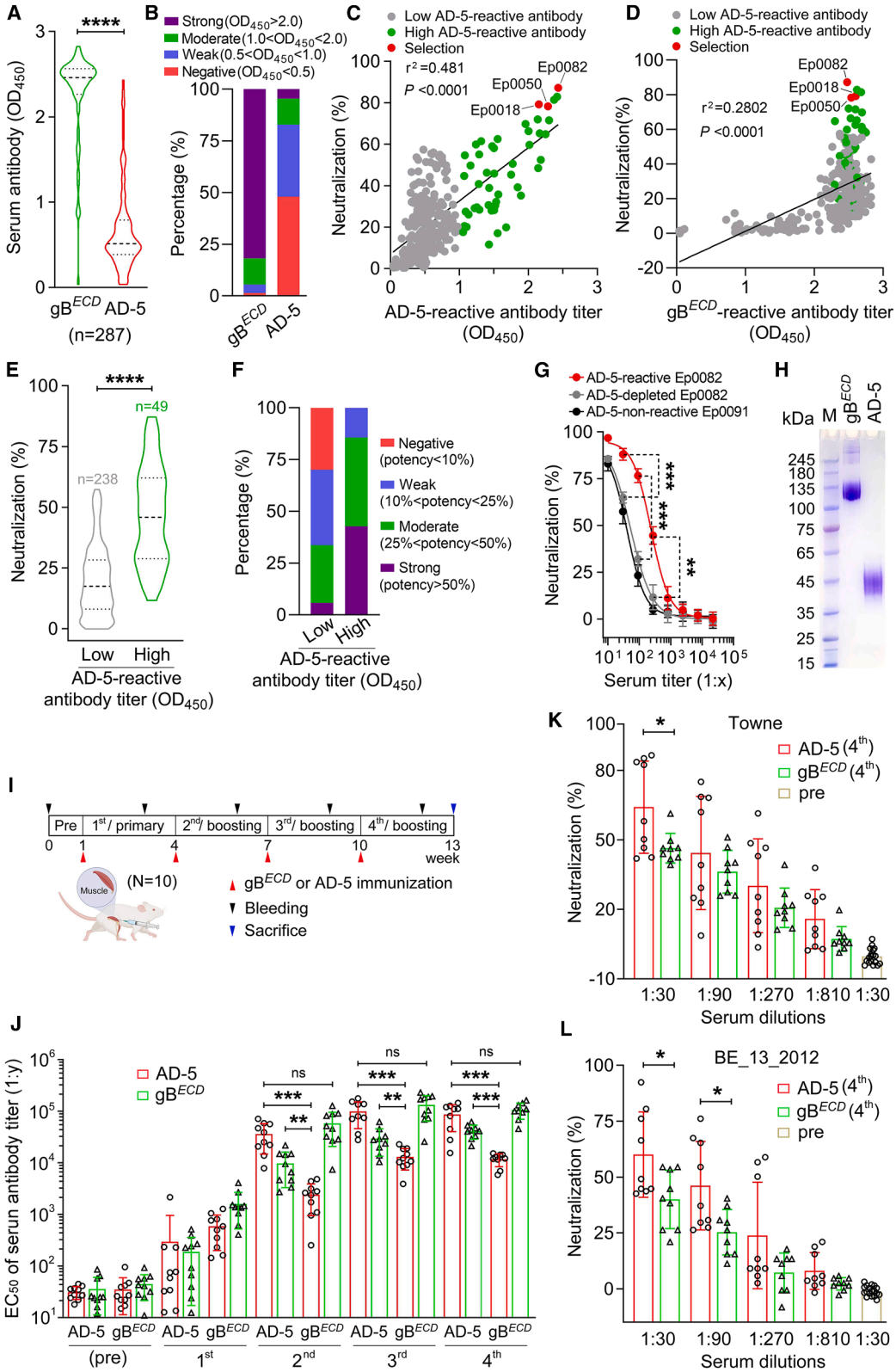


*(legend on next page)*

compared the immunogenicity of recombinant AD-5 and gB$^{ECD}$ proteins in mice using a prime-and-boost strategy (Figures 6H and 6I). Serum binding antibody titers, assessed by ELISA, showed that both proteins elicited comparable titers of binding antibodies post-immunization (Figure 6J). However, AD-5 induced significantly higher AD-5-reactive antibody titers than gB$^{ECD}$ following boost immunizations (Figure 6J), underscoring its immunodominance of AD-5-focused immunization. Additionally, AD-5-immunized sera exhibited significantly higher neutralizing titers against the Towne and BE13/2012 strains compared to gB$^{ECD}$-immunized sera (Figures 6K and 6L). Of note, AD-5-immunized serum displayed greater variability in nAb titers, with almost half of the samples exhibiting improved nAb titers (Figures 6K and 6L). This suggests that optimizing the AD-5 immunogen is necessary to achieve more consistent and enhanced antibody responses. Collectively, these findings indicate that AD-5 could serve as a superior immunogen for inducing focused and potent nAbs compared to gB$^{ECD}$.

## DISCUSSION

hCMV is a prevalent pathogen responsible for severe CMV diseases and complications in immunocompromised individuals. However, progress in developing effective hCMV vaccines and antibody therapeutics has been limited. Concerns about the lack of a direct correlation between nAbs and clinical benefits have arisen regarding antibody therapies.[20,21,45] Nonetheless, studies indicate that antibodies or HIGs can provide certain clinical protection to CMV-negative pregnant women and organ transplant patients.[5,29,30,46] Therefore, it is crucial to develop highly potent hCMV antibodies for improved clinical protection. hCMV gB plays a critical role in viral entry and is a key target for vaccine and therapeutic antibody development.[47] In this study, we systematically analyzed gB-specific antibody profiles from 3 individuals with latent-infected hCMV and identified highly potent cluster I nAbs that competitively recognize a unique epitope on AD-5. Cluster I nAbs originate from diverse clonal lineages, suggesting that the germline repertoire is readily available for initiating and developing this type of nAbs in response to vaccination.

Cryo-EM structure analysis revealed a highly exposed and conserved neutralizing epitope on AD-5. Homology modeling of the AD-5/cluster I nAbs demonstrated commonality among the epitopes, which might be the structural basis for cluster I nAbs to perform similar biological functions. This epitope commonality could serve as a structural basis for designing vaccines to orientally induce diverse and effective antibodies.

Glycosylation modifications in the viral envelope enable evasion of host immune surveillance.[48–50] hCMV gB is extensively shielded by a dense layer of glycans,[34] particularly at highly efficient neutralizing epitopes (e.g., Asn383 for the SM5-1 epitope on AD-4 and Asn281 for the 1G2 epitope on AD-5).[34,36] However, glycopeptide analysis indicates that the newly identified epitope is unmodified by glycosylation, highlighting its exposed nature. This finding might explain its ability to induce diverse germline-derived antibody responses.

Three hypotheses explain the neutralizing mechanisms of antibodies targeting hCMV gB. First, the antibody might block gB-mediated viral adsorption to receptors such as heparan sulfate proteoglycans (HSPGs) and integrin-β.[41,51–53] However, studies have shown that none of the identified nAbs, including our cluster I nAbs, act via this mode. Second, antibodies could interfere with the core fusion apparatus composed of gB and the gH/gL heterodimer.[54–56] However, the formation of this apparatus occurs independently of receptor binding or membrane fusion, as gB and gH/gL form stable complexes in the endoplasmic reticulum.[57,58] Thus, there is no opportunity for antibody intervention. Third, antibodies might inhibit the

**Figure 6. Analysis of immunogenicity and neutralizing activity of serum from natural infections (human) and passive immunization (mice)**

(A) Serological binding antibodies to gB$^{ECD}$ and AD-5 antigens were assessed in 287 human serum samples using ELISA. Data are represented as mean ± SD. Statistical analysis was performed using a two-tailed unpaired t test (****$p < 0.0001$).

(B) Proportion of serum samples with varying degrees of immunoreactivity against AD-5 and gB$^{ECD}$. $OD_{450}$ values were measured by ELISA using a 1:1,000 serum dilution.

(C and D) Correlation analysis of AD-5- and gB$^{ECD}$-reactive antibody titers with serum neutralization activity. Serum samples with high (green dots, $OD_{450} > 1.0$ at 1:1,000 dilution) and low (gray dots, $OD_{450} < 1.0$ at 1:1,000 dilution) AD-5-reactive antibody titers were plotted versus the results of the heat-inactivated serum neutralization assays at a 1:50 dilution against Towne strain in MRC-5 cells. Significance was assessed using Pearson's correlations. Samples with high AD-5-reactive antibody titers and strong neutralizing activity (>50%) selected for antibody analysis in this study are highlighted in red.

(E) Comparison of neutralization activity of serum samples with high ($n = 49$) and low ($n = 238$) AD-5-reactive antibody titers. Statistical analysis was performed using a two-tailed unpaired t test (****$p < 0.0001$).

(F) Proportion of serum samples with various levels of neutralizing potency against the Towne strain in MRC-5 cells, categorized by high ($OD_{450} > 1.0$) and low ($OD_{450} < 1.0$) AD-5-reactive antibody titers. $OD_{450}$ values were measured by ELISA at a 1:1,000 serum dilution.

(G) Comparison of neutralization activity of AD-5-reactive serum sample (Es0082) and its corresponding AD-5 antibody-depleted sample, as well as AD-5-non-reactive serum sample (Es0091). AD-5-reactive antibodies were depleted using saturated amounts of recombinant soluble AD-5 protein. Data are represented as mean ± SEM. Representative results from at least two independent experiments are shown. Statistical analysis was performed using a two-tailed unpaired t test (**$p < 0.01$ and ***$p < 0.001$).

(H) Expression and purification of recombinant gB$^{ECD}$ and AD-5 proteins in Expi293F, followed by affinity chromatography using a 6-histidine tag. Purified proteins were used for mice immunization.

(I) Immunization schedule for mice receiving purified recombinant gB$^{ECD}$ and AD-5 proteins, with serum samples collected at specified time points. Pre-immune (pre) and post-immune sera were collected after each of 4 immunizations for binding and neutralization assays.

(J) Binding antibody titers to AD-5 and gB$^{ECD}$ of in post-immune sera, assayed by ELISA. The *y* axis represents serum antibody titers. Data are represented as mean ± SD ($n = 10$ or 9 mice per group). Statistical analysis was performed using a two-tailed unpaired t test (**$p < 0.01$, ***$p < 0.001$, and ns, not significant).

(K and L) Neutralization activity of mouse sera after the 4$^{th}$ immunization against the Towne and BE13/2012 strains. Data are represented as mean ± SD ($n = 9$ mice per group). Statistical analysis was performed using a two-tailed unpaired t test (*$p < 0.05$).

transition of gB from its prefusion to postfusion conformation. Notably, approximately 25% of gB in virions is in the postfusion state,[58] and antibodies in this study bind well to gB in both conformations, leaving this hypothesis uncertain. In contrast, our study demonstrates that 1B03 specifically targets the fusion subdomain of gB, which contains two fusion loops. The steric hindrance or allosteric effects induced by 1B03 might disrupt the fusion-loop-triggered membrane fusion. The significantly superior efficacy of 1B03 against viral initial infection and cell-to-cell spread compared to reference nAbs might be attributed to its unique antigenic epitopes. Furthermore, the epitope peptide of 1B03 shows high homology and conservation among various strains (Figure S10), suggesting a broad neutralizing spectrum.

In general, over 90% of antibodies against gB elicited by natural infection or vaccination are non-neutralizing,[17,34] potentially diminishing the efficacy of nAbs through epitope competition or promoting antibody-dependent enhancement of hCMV infection.[40,59,60] The serologic response to gB does not accurately reflect the efficacy of hCMV gB vaccines. Therefore, long-term and effective immune protection from hCMV gB vaccination might depend significantly on the levels of induced nAb titers. Optimizing hCMV gB vaccines to focus the immune response on critical neutralizing domain(s) (e.g., AD-4 and AD-5) while reducing ineffective responses could be beneficial. The monomeric form of AD-5 elicits a robust immune response and enhances neutralization capabilities. Incorporating AD-5 into a ferritin nanoparticle has proven successful for this vaccination strategy.[61] This study explores the structural basis of AD-5 for vaccine development, highlighting multiple vulnerable sites that elicit potent nAbs. Therefore, designing and optimizing the hCMV gB vaccine based on the AD-5 structure is a viable approach.

hCMV transmission primarily occurs via viremia and cell-to-cell spread *in vivo*.[24] Previous clinical efforts to avert hCMV infection in posttransplant and pregnancy scenarios have yielded controversial results,[6,29] as antibody therapies have shown antiviral activity without a direct correlation to anticipated protection.[20,62,63] This might be attributed to the inability of antibodies to effectively suppress viral cell-to-cell spread, the main mode of tissue infection.[27,64] The GB/MF59 vaccine induces non-neutralizing antibodies that facilitate virion phagocytosis and prevent cell-to-cell spread of hCMV, correlating with the observed clinical protection in seronegative postpartum women and transplant recipients.[21,45] These findings underscore the necessity for antibodies to possess diverse biological functions to combat hCMV. In addition to potently neutralizing cell-free virions, 1B03-like antibodies can effectively block viral cell-to-cell spread and impact viral growth in cells, reducing the risk of re-infection. Moreover, cytologic effects mediated by immune cells (e.g., monocytes or effector T cells) on antibody-bound viruses are associated with a decreased risk of congenital hCMV infection and placental hCMV transmission.[65–67] Consistently, 1B03 exhibits significant ADCC, ADCP, and CDC effects, suggesting that these effects might be helpful for eliminating early CMV-reactivated and newly infected cells, leading to virus clearance *in vivo*. Given their diverse and effective biological functions, 1B03-like antibodies likely play a crucial role in humoral immunity against hCMV in healthy individuals. Therefore, it is essential for vaccines to include antigenic epitopes that can induce such antibodies.

In conclusion, we identified a cluster of potent nAbs that competitively target a previously uncharacterized epitope on gB AD-5. These antibodies might be pivotal to humoral immunity in effectively controlling hCMV and represent a promising option for antibody-based therapeutics. Moreover, our insights into epitope characterization and the functional mechanisms of nAbs enhance our understanding of the host humoral immune response to hCMV gB, providing a solid foundation for developing efficient therapeutic agents and advanced gB-based vaccines against hCMV.

## Limitations of the study

Our study identified a panel of potent nAbs (cluster I nAbs) targeting previously uncharacterized epitopes in hCMV gB from three selected top neutralizers. While cluster I nAbs exhibit exceptional neutralization *in vitro*, their broader prevalence across the hCMV-seropositive population remains to be established through comprehensive epidemiological studies in diverse cohorts, which is crucial for broadly assessing the protective efficacy of humoral immunity. Moreover, cryo-EM structural analysis only resolved the gB-1B03 complex architecture. Although homology modeling revealed conserved epitope features among cluster I nAbs, this computational approach cannot substitute for experimental determination. Therefore, structural characterization of other gB-mAb complexes using cryo-EM or X-ray crystallography is essential to elucidate precise binding topologies and neutralization mechanisms. Finally, we have not yet tested the cluster I nAbs *in vivo*, which is an important step in successfully translating candidates for clinical applications.

## RESOURCE AVAILABILITY

### Lead contact

Further information and requests for resources and reagents should be directed to and will be fulfilled by the lead contact, Hua-Xin Liao (larryhliao@trinomab.com).

### Materials availability

All unique and stable reagents generated in this study are available via the lead contact upon reasonable request.

### Data and code availability

The cryo-EM structure has been deposited to the Protein Data Bank and is publicly available as of the date of publication. Accession numbers are listed in the key resources table. Any additional information required to reanalyze the data reported in this paper is available from the lead contact upon a reasonable request.

## ACKNOWLEDGMENTS

We would like to thank Prof. Hua Zhu, Zhikang Qian, and Mingli Wang for providing virus strains. Cryo-EM data were collected at the Cryo-EM Facility in Shanghai, and cryo-EM samples were prepared and optimized at the Instrumental Analysis Center of Xi'an Jiaotong University. This work was supported by the Guangdong Innovative and Entrepreneurial Research Team Program (no. 2013Y113), the Guangdong Natural Science Foundation Project Fundamental and Applied Fundamental Research Fund (no. 2114050001966), and the Zhuhai Innovative and Entrepreneurial Research Team Program (no. ZH01110405160015PWC).

## AUTHOR CONTRIBUTIONS

C.W. designed the study; C.W., Y.A., Yayu Wang, and D.K.J. performed the research; N.S., Y.Z., H.W., L.Z., Z.Y., and S.Z. performed and analyzed the structural data; C.W., Yueming Wang, T.L., N.L., X.Y., C.L., and W.Z. analyzed the data; H.-X.L. designed and directed the study, analyzed the data, and supervised the overall work; and C.W. and H.-X.L. wrote and edited the paper. C. W., who was a PhD student, performed the initial characterization of the antibodies isolated by the hCMV study team of Trinomab as directed by H.-X.L., who served as a faculty member and mentor at the time at Jinan University. All authors have read and approved the article.

## DECLARATION OF INTERESTS

Yueming Wang, W.Z., and H.-X.L. have patent applications on the nAbs used in this study.

## STAR★METHODS

Detailed methods are provided in the online version of this paper and include the following:

- KEY RESOURCES TABLE
- EXPERIMENTAL MODEL AND STUDY PARTICIPANT DETAILS
  - Human blood sample collection
  - Cells and viruses
  - Mice
- METHOD DETAILS
  - hCMV antigens
  - Single B cell sorting and cloning of antibody variable genes
  - Expression and purification of recombinant IgG and Fab
  - Virus neutralization assays
  - ELISA assays for cross-competitive binding
  - Immunoprecipitation of hCMV virion with antibodies
  - Virus adsorption and effect of antibodies on virus entry
  - Inhibition assays for cell-to-cell spread of hCMV
  - Antibody-mediated ADCC, ADCP and CDC assays
  - Detection of antibodies entered the cells by immunofluorescence
  - Passages of hCMV virus with antibody
  - Characterization of the molecular basis of antibody biological functions
  - Biochemical and FSEC analysis
  - Cryo-EM sample preparation
  - Cryo-EM data collection and processing
  - Atomic model building and refinement
  - Model construction of antigen-antibody interaction
  - Binding affinity of antibody to hCMV gB or mutants by SPR
  - Epitope cross-competitive assay by SPR
  - Structural analysis of N-glycosylation of hCMV gB AD-5
  - Deglycosylation of gB
  - Human serum neutralization assays
  - Mouse immunization and serum neutralization
- QUANTIFICATION AND STATISTICAL ANALYSIS

## SUPPLEMENTAL INFORMATION

Supplemental information can be found online at https://doi.org/10.1016/j.celrep.2025.115646.

Received: November 4, 2024
Revised: February 25, 2025
Accepted: April 11, 2025
Published: May 17, 2025

## REFERENCES

1. Fisher, S., Genbacev, O., Maidji, E., and Pereira, L. (2000). Human cytomegalovirus infection of placental cytotrophoblasts in vitro and in utero: implications for transmission and pathogenesis. J. Virol. *74*, 6808–6820. https://doi.org/10.1128/jvi.74.15.6808-6820.2000.
2. Kenneson, A., and Cannon, M.J. (2007). Review and meta-analysis of the epidemiology of congenital cytomegalovirus (CMV) infection. Rev. Med. Virol. *17*, 253–276. https://doi.org/10.1002/rmv.535.
3. Vogel, J.U., Otte, J., Koch, F., Gümbel, H., Doerr, H.W., and Cinatl, J., Jr. (2013). Role of human cytomegalovirus genotype polymorphisms in AIDS patients with cytomegalovirus retinitis. Med. Microbiol. Immunol. *202*, 37–47. https://doi.org/10.1007/s00430-012-0244-3.
4. Griffiths, P., Baraniak, I., and Reeves, M. (2015). The pathogenesis of human cytomegalovirus. J. Pathol. *235*, 288–297. https://doi.org/10.1002/path.4437.
5. Adler, S.P., and Nigro, G. (2009). Findings and conclusions from CMV hyperimmune globulin treatment trials. J. Clin. Virol. *46*, S54–S57. https://doi.org/10.1016/j.jcv.2009.08.017.
6. Nigro, G. (2017). Hyperimmune globulin in pregnancy for the prevention of congenital cytomegalovirus disease. Expert Rev. Anti Infect. Ther. *15*, 977–986. https://doi.org/10.1080/14787210.2017.1398081.
7. Hakki, M. (2020). Moving Past Ganciclovir and Foscarnet: Advances in CMV Therapy. Curr. Hematol. Malig. Rep. *15*, 90–102. https://doi.org/10.1007/s11899-020-00557-6.
8. Morillo-Gutierrez, B., Waugh, S., Pickering, A., Flood, T., and Emonts, M. (2017). Emerging (val)ganciclovir resistance during treatment of congenital CMV infection: a case report and review of the literature. BMC Pediatr. *17*, 181. https://doi.org/10.1186/s12887-017-0933-6.
9. Douglas, C.M., Barnard, R., Holder, D., Leavitt, R., Levitan, D., Maguire, M., Nickle, D., Teal, V., Wan, H., van Alewijk, D.C.J.G., et al. (2020). Letermovir resistance analysis in a clinical trial of cytomegalovirus prophylaxis for hematopoietic stem cell transplant recipients. J. Infect. Dis. *221*, 1117–1126. https://doi.org/10.1093/infdis/jiz577.
10. Hofmann, E., Sidler, D., Dahdal, S., Bittel, P., Suter-Riniker, F., Manuel, O., Walti, L.N., and Hirzel, C. (2021). Emergence of letermovir resistance in solid organ transplant recipients with ganciclovir resistant cytomegalovirus infection: A case series and review of the literature. Transpl. Infect. Dis. *23*, e13515. https://doi.org/10.1111/tid.13515.
11. Nguyen, C.C., and Kamil, J.P. (2018). Pathogen at the Gates: Human Cytomegalovirus Entry and Cell Tropism. Viruses *10*, 704. https://doi.org/10.3390/v10120704.
12. Kabanova, A., Marcandalli, J., Zhou, T., Bianchi, S., Baxa, U., Tsybovsky, Y., Lilleri, D., Silacci-Fregni, C., Foglierini, M., Fernandez-Rodriguez, B.M., et al. (2016). Platelet-derived growth factor-alpha receptor is the cellular receptor for human cytomegalovirus gHgLgO trimer. Nat. Microbiol. *1*, 16082. https://doi.org/10.1038/nmicrobiol.2016.82.
13. Martinez-Martin, N., Marcandalli, J., Huang, C.S., Arthur, C.P., Perotti, M., Foglierini, M., Ho, H., Dosey, A.M., Shriver, S., Payandeh, J., et al. (2018). An Unbiased Screen for Human Cytomegalovirus Identifies Neuropilin-2 as a Central Viral Receptor. Cell *174*, 1158–1171.e19. https://doi.org/10.1016/j.cell.2018.06.028.
14. Harrison, S.C. (2008). Viral membrane fusion. Nat. Struct. Mol. Biol. *15*, 690–698. https://doi.org/10.1038/nsmb.1456.
15. Isaacson, M.K., and Compton, T. (2009). Human cytomegalovirus glycoprotein B is required for virus entry and cell-to-cell spread but not for virion attachment, assembly, or egress. J. Virol. *83*, 3891–3903. https://doi.org/10.1128/JVI.01251-08.
16. Zydek, M., Petitt, M., Fang-Hoover, J., Adler, B., Kauvar, L.M., Pereira, L., and Tabata, T. (2014). HCMV infection of human trophoblast progenitor cells of the placenta is neutralized by a human monoclonal antibody to glycoprotein B and not by antibodies to the pentamer complex. Viruses *6*, 1346–1364. https://doi.org/10.3390/v6031346.
17. Pötzsch, S., Spindler, N., Wiegers, A.K., Fisch, T., Rücker, P., Sticht, H., Grieb, N., Baroti, T., Weisel, F., Stamminger, T., et al. (2011). B cell repertoire analysis identifies new antigenic domains on glycoprotein B of human

cytomegalovirus which are target of neutralizing antibodies. PLoS Pathog. *7*, e1002172. https://doi.org/10.1371/journal.ppat.1002172.

18. Pass, R.F., Zhang, C., Evans, A., Simpson, T., Andrews, W., Huang, M.L., Corey, L., Hill, J., Davis, E., Flanigan, C., and Cloud, G. (2009). Vaccine prevention of maternal cytomegalovirus infection. N. Engl. J. Med. *360*, 1191–1199. https://doi.org/10.1056/NEJMoa0804749.
19. Baraniak, I., Gomes, A.C., Sodi, I., Langstone, T., Rothwell, E., Atkinson, C., Pichon, S., Piras-Douce, F., Griffiths, P.D., and Reeves, M.B. (2019). Seronegative patients vaccinated with cytomegalovirus gB-MF59 vaccine have evidence of neutralising antibody responses against gB early post-transplantation. EBioMedicine *50*, 45–54. https://doi.org/10.1016/j.ebiom.2019.11.005.
20. Goodwin, M.L., Webster, H.S., Wang, H.Y., Jenks, J.A., Nelson, C.S., Tu, J.J., Mangold, J.F., Valencia, S., Pollara, J., Edwards, W., et al. (2020). Specificity and effector functions of non-neutralizing gB-specific monoclonal antibodies isolated from healthy individuals with human cytomegalovirus infection. Virology *548*, 182–191. https://doi.org/10.1016/j.virol.2020.07.009.
21. Gomes, A.C., Baraniak, I.A., Lankina, A., Moulder, Z., Holenya, P., Atkinson, C., Tang, G., Mahungu, T., Kern, F., Griffiths, P.D., and Reeves, M. B. (2023). The cytomegalovirus gB/MF59 vaccine candidate induces antibodies against an antigenic domain controlling cell-to-cell spread. Nat. Commun. *14*, 1041. https://doi.org/10.1038/s41467-023-36683-x.
22. Cui, X., Freed, D.C., Wang, D., Qiu, P., Li, F., Fu, T.M., Kauvar, L.M., and McVoy, M.A. (2017). Impact of Antibodies and Strain Polymorphisms on Cytomegalovirus Entry and Spread in Fibroblasts and Epithelial Cells. J. Virol. *91*, e01650-16–e01616. https://doi.org/10.1128/JVI.01650-16.
23. Ai, Y., Wu, C., Zhang, M., Jaijyan, D.K., Liu, T., Zan, L., Li, N., Yu, W., Wang, Y., Yuan, X., et al. (2022). Neutralization Epitopes in Trimer and Pentamer Complexes Recognized by Potent Cytomegalovirus-Neutralizing Human Monoclonal Antibodies. Microbiol. Spectr. *10*, e0139322. https://doi.org/10.1128/spectrum.01393-22.
24. Reuter, N., Kropff, B., Britt, W.J., Mach, M., and Thomas, M. (2022). Neutralizing Antibodies Limit Cell-Associated Spread of Human Cytomegalovirus in Epithelial Cells and Fibroblasts. Viruses *14*, 284. https://doi.org/10.3390/v14020284.
25. Maertens, J., Logan, A.C., Jang, J., Long, G., Tang, J.L., Hwang, W.Y.K., Koh, L.P., Chemaly, R., Gerbitz, A., Winkler, J., et al. (2020). Phase 2 Study of Anti-Human Cytomegalovirus Monoclonal Antibodies for Prophylaxis in Hematopoietic Cell Transplantation. Antimicrob. Agents Chemother. *64*, e02467-19. https://doi.org/10.1128/AAC.02467-19.
26. Ishida, J.H., Patel, A., Mehta, A.K., Gatault, P., McBride, J.M., Burgess, T., Derby, M.A., Snydman, D.R., Emu, B., Feierbach, B., et al. (2017). Phase 2 Randomized, Double-Blind, Placebo-Controlled Trial of RG7667, a Combination Monoclonal Antibody, for Prevention of Cytomegalovirus Infection in High-Risk Kidney Transplant Recipients. Antimicrob. Agents Chemother. *61*, e01794-16. https://doi.org/10.1128/aac.01794-16.
27. Falk, J.J., Winkelmann, M., Sampaio, K.L., Paal, C., Schrezenmeier, H., Alt, M., Stanton, R., Krawczyk, A., Lotfi, R., and Sinzger, C. (2018). Large-Scale Screening of HCMV-Seropositive Blood Donors Indicates that HCMV Effectively Escapes from Antibodies by Cell-Associated Spread. Viruses *10*, 500. https://doi.org/10.3390/v10090500.
28. Furione, M., Rognoni, V., Sarasini, A., Zavattoni, M., Lilleri, D., Gerna, G., and Revello, M.G. (2013). Slow increase in IgG avidity correlates with prevention of human cytomegalovirus transmission to the fetus. J. Med. Virol. *85*, 1960–1967. https://doi.org/10.1002/jmv.23691.
29. Bonaros, N., Mayer, B., Schachner, T., Laufer, G., and Kocher, A. (2008). CMV-hyperimmune globulin for preventing cytomegalovirus infection and disease in solid organ transplant recipients: a meta-analysis. Clin. Transplant. *22*, 89–97. https://doi.org/10.1111/j.1399-0012.2007.00750.x.
30. Rea, F., Potena, L., Yonan, N., Wagner, F., and Calabrese, F. (2016). Cytomegalovirus Hyper Immunoglobulin for CMV Prophylaxis in Thoracic Transplantation. Transplantation *100*, S19–S26. https://doi.org/10.1097/TP.0000000000001096.
31. Griffiths, P., and Reeves, M. (2021). Pathogenesis of human cytomegalovirus in the immunocompromised host. Nat. Rev. Microbiol. *19*, 759–773. https://doi.org/10.1038/s41579-021-00582-z.
32. Heldwein, E.E., Lou, H., Bender, F.C., Cohen, G.H., Eisenberg, R.J., and Harrison, S.C. (2006). Crystal structure of glycoprotein B from herpes simplex virus 1. Science *313*, 217–220. https://doi.org/10.1126/science.1126548.
33. Backovic, M., Longnecker, R., and Jardetzky, T.S. (2009). Structure of a trimeric variant of the Epstein-Barr virus glycoprotein B. Proc. Natl. Acad. Sci. USA *106*, 2880–2885. https://doi.org/10.1073/pnas.0810530106.
34. Burke, H.G., and Heldwein, E.E. (2015). Crystal Structure of the Human Cytomegalovirus Glycoprotein B. PLoS Pathog. *11*, e1005227. https://doi.org/10.1371/journal.ppat.1005227.
35. Spindler, N., Diestel, U., Stump, J.D., Wiegers, A.K., Winkler, T.H., Sticht, H., Mach, M., and Muller, Y.A. (2014). Structural basis for the recognition of human cytomegalovirus glycoprotein B by a neutralizing human antibody. PLoS Pathog. *10*, e1004377. https://doi.org/10.1371/journal.ppat.1004377.
36. Chandramouli, S., Ciferri, C., Nikitin, P.A., Caló, S., Gerrein, R., Balabanis, K., Monroe, J., Hebner, C., Lilja, A.E., Settembre, E.C., and Carfi, A. (2015). Structure of HCMV glycoprotein B in the postfusion conformation bound to a neutralizing human antibody. Nat. Commun. *6*, 8176. https://doi.org/10.1038/ncomms9176.
37. Liu, Y., Heim, K.P., Che, Y., Chi, X., Qiu, X., Han, S., Dormitzer, P.R., and Yang, X. (2021). Prefusion structure of human cytomegalovirus glycoprotein B and structural basis for membrane fusion. Sci. Adv. *7*, eabf3178. https://doi.org/10.1126/sciadv.abf3178.
38. Thomson, C.A., Bryson, S., McLean, G.R., Creagh, A.L., Pai, E.F., and Schrader, J.W. (2008). Germline V-genes sculpt the binding site of a family of antibodies neutralizing human cytomegalovirus. EMBO J. *27*, 2592–2602. https://doi.org/10.1038/emboj.2008.179.
39. Eisenberg, R.J., Cairns, T.M., and Cohen, G.H. (2011). HCMV grabs a mechanism to escape neutralization. Cell Host Microbe *10*, 177–178. https://doi.org/10.1016/j.chom.2011.08.011.
40. Manley, K., Anderson, J., Yang, F., Szustakowski, J., Oakeley, E.J., Compton, T., and Feire, A.L. (2011). Human cytomegalovirus escapes a naturally occurring neutralizing antibody by incorporating it into assembling virions. Cell Host Microbe *10*, 197–209. https://doi.org/10.1016/j.chom.2011.07.010.
41. Compton, T., Nowlin, D.M., and Cooper, N.R. (1993). Initiation of human cytomegalovirus infection requires initial interaction with cell surface heparan sulfate. Virology *193*, 834–841. https://doi.org/10.1006/viro.1993.1192.
42. Vezzani, G., Pimazzoni, S., Ferranti, R., Calò, S., Monda, G., Amendola, D., Frigimelica, E., Maione, D., Cortese, M., and Merola, M. (2022). Human immunoglobulins are transported to HCMV viral envelope by viral Fc gamma receptors-dependent and independent mechanisms. Front. Microbiol. *13*, 1106401. https://doi.org/10.3389/fmicb.2022.1106401.
43. Webb, B., and Sali, A. (2016). Comparative Protein Structure Modeling Using MODELLER. Curr. Protoc. Bioinformatics *54*, 5.6.1–5.6.37. https://doi.org/10.1002/cpbi.3.
44. Schoppel, K., Kropff, B., Schmidt, C., Vornhagen, R., and Mach, M. (1997). The humoral immune response against human cytomegalovirus is characterized by a delayed synthesis of glycoprotein-specific antibodies. J. Infect. Dis. *175*, 533–544. https://doi.org/10.1093/infdis/175.3.533.
45. Nelson, C.S., Huffman, T., Jenks, J.A., Cisneros de la Rosa, E., Xie, G., Vandergrift, N., Pass, R.F., Pollara, J., and Permar, S.R. (2018). HCMV glycoprotein B subunit vaccine efficacy mediated by nonneutralizing antibody effector functions. Proc. Natl. Acad. Sci. USA *115*, 6267–6272. https://doi.org/10.1073/pnas.1800177115.
46. Alsuliman, T., Kitel, C., Dulery, R., Guillaume, T., Larosa, F., Cornillon, J., Labussière-Wallet, H., Médiavilla, C., Belaiche, S., Delage, J., et al. (2018). Cytotect®CP as salvage therapy in patients with CMV infection following

allogeneic hematopoietic cell transplantation: a multicenter retrospective study. Bone Marrow Transplant. *53*, 1328–1335. https://doi.org/10.1038/s41409-018-0166-9.

47. Wang, D., and Fu, T.M. (2014). Progress on human cytomegalovirus vaccines for prevention of congenital infection and disease. Curr. Opin. Virol. *6*, 13–23. https://doi.org/10.1016/j.coviro.2014.02.004.
48. Gavrilov, B.K., Rogers, K., Fernandez-Sainz, I.J., Holinka, L.G., Borca, M. V., and Risatti, G.R. (2011). Effects of glycosylation on antigenicity and immunogenicity of classical swine fever virus envelope proteins. Virology *420*, 135–145. https://doi.org/10.1016/j.virol.2011.08.025.
49. Ma, B.J., Alam, S.M., Go, E.P., Lu, X., Desaire, H., Tomaras, G.D., Bowman, C., Sutherland, L.L., Scearce, R.M., Santra, S., et al. (2011). Envelope deglycosylation enhances antigenicity of HIV-1 gp41 epitopes for both broad neutralizing antibodies and their unmutated ancestor antibodies. PLoS Pathog. *7*, e1002200. https://doi.org/10.1371/journal.ppat.1002200.
50. Liu, P., Yue, C., Meng, B., Xiao, T., Yang, S., Liu, S., Jian, F., Zhu, Q., Yu, Y., Ren, Y., et al. (2024). Spike N354 glycosylation augments SARS-CoV-2 fitness for human adaptation through structural plasticity. Natl. Sci. Rev. *11*, nwae206. https://doi.org/10.1093/nsr/nwae206.
51. Boyle, K.A., and Compton, T. (1998). Receptor-binding properties of a soluble form of human cytomegalovirus glycoprotein B. J. Virol. *72*, 1826–1833. https://doi.org/10.1128/JVI.72.3.1826-1833.1998.
52. Feire, A.L., Koss, H., and Compton, T. (2004). Cellular integrins function as entry receptors for human cytomegalovirus via a highly conserved disintegrin-like domain. Proc. Natl. Acad. Sci. USA *101*, 15470–15475. https://doi.org/10.1073/pnas.0406821.
53. Feire, A.L., Roy, R.M., Manley, K., and Compton, T. (2010). The glycoprotein B disintegrin-like domain binds beta 1 integrin to mediate cytomegalovirus entry. J. Virol. *84*, 10026–10037. https://doi.org/10.1128/JVI.00710-10.
54. Avitabile, E., Forghieri, C., and Campadelli-Fiume, G. (2009). Cross talk among the glycoproteins involved in herpes simplex virus entry and fusion: the interaction between gB and gH/gL does not necessarily require gD. J. Virol. *83*, 10752–10760. https://doi.org/10.1128/JVI.01287-09.
55. Gianni, T., Amasio, M., and Campadelli-Fiume, G. (2009). Herpes simplex virus gD forms distinct complexes with fusion executors gB and gH/gL in part through the C-terminal profusion domain. J. Biol. Chem. *284*, 17370–17382. https://doi.org/10.1074/jbc.M109.005728.
56. Cairns, T.M., Whitbeck, J.C., Lou, H., Heldwein, E.E., Chowdary, T.K., Eisenberg, R.J., and Cohen, G.H. (2011). Capturing the herpes simplex virus core fusion complex (gB-gH/gL) in an acidic environment. J. Virol. *85*, 6175–6184. https://doi.org/10.1128/JVI.00119-11.
57. Vanarsdall, A.L., Howard, P.W., Wisner, T.W., and Johnson, D.C. (2016). Human Cytomegalovirus gH/gL Forms a Stable Complex with the Fusion Protein gB in Virions. PLoS Pathog. *12*, e1005564. https://doi.org/10.1371/journal.ppat.1005564.
58. Si, Z., Zhang, J., Shivakoti, S., Atanasov, I., Tao, C.L., Hui, W.H., Zhou, K., Yu, X., Li, W., Luo, M., et al. (2018). Different functional states of fusion protein gB revealed on human cytomegalovirus by cryo electron tomography with Volta phase plate. PLoS Pathog. *14*, e1007452. https://doi.org/10.1371/journal.ppat.1007452.
59. Maidji, E., McDonagh, S., Genbacev, O., Tabata, T., and Pereira, L. (2006). Maternal antibodies enhance or prevent cytomegalovirus infection in the placenta by neonatal Fc receptor-mediated transcytosis. Am. J. Pathol. *168*, 1210–1226. https://doi.org/10.2353/ajpath.2006.050482.
60. Gardner, T.J., and Tortorella, D. (2016). Virion Glycoprotein-Mediated Immune Evasion by Human Cytomegalovirus: a Sticky Virus Makes a Slick Getaway. Microbiol. Mol. Biol. Rev. *80*, 663–677. https://doi.org/10.1128/MMBR.00018-16.
61. Perotti, M., Marcandalli, J., Demurtas, D., Sallusto, F., and Perez, L. (2020). Rationally designed Human Cytomegalovirus gB nanoparticle vaccine with improved immunogenicity. PLoS Pathog. *16*, e1009169. https://doi.org/10.1371/journal.ppat.1009169.
62. Baraniak, I., Kropff, B., Ambrose, L., McIntosh, M., McLean, G.R., Pichon, S., Atkinson, C., Milne, R.S.B., Mach, M., Griffiths, P.D., and Reeves, M.B. (2018). Protection from cytomegalovirus viremia following glycoprotein B vaccination is not dependent on neutralizing antibodies. Proc. Natl. Acad. Sci. USA *115*, 6273–6278. https://doi.org/10.1073/pnas.1800224115.
63. Lilleri, D., Zelini, P., Fornara, C., Zavaglio, F., Rampino, T., Perez, L., Gabanti, E., and Gerna, G. (2018). Human cytomegalovirus (HCMV)-specific T cell but not neutralizing or IgG binding antibody responses to glycoprotein complexes gB, gHgLgO, and pUL128L correlate with protection against high HCMV viral load reactivation in solid-organ transplant recipients. J. Med. Virol. *90*, 1620–1628. https://doi.org/10.1002/jmv.25225.
64. Zehner, M., Alt, M., Ashurov, A., Goldsmith, J.A., Spies, R., Weiler, N., Lerma, J., Gieselmann, L., Stöhr, D., Gruell, H., et al. (2023). Single-cell analysis of memory B cells from top neutralizers reveals multiple sites of vulnerability within HCMV Trimer and Pentamer. Immunity *56*, 2602–2620.e10. https://doi.org/10.1016/j.immuni.2023.10.009.
65. Semmes, E.C., Miller, I.G., Wimberly, C.E., Phan, C.T., Jenks, J.A., Harnois, M.J., Berendam, S.J., Webster, H., Hurst, J.H., Kurtzberg, J., et al. (2022). Maternal Fc-mediated non-neutralizing antibody responses correlate with protection against congenital human cytomegalovirus infection. J. Clin. Investig. *132*, e156827. https://doi.org/10.1172/jci156827.
66. Mihalić, A., Železnjak, J., Lisnić, B., Jonjić, S., Juranić Lisnić, V., and Brizić, I. (2024). Immune surveillance of cytomegalovirus in tissues. Cell. Mol. Immunol. *21*, 959–981. https://doi.org/10.1038/s41423-024-01186-2.
67. Rolin, C., Zimmer, J., and Seguin-Devaux, C. (2024). Bridging the gap with multispecific immune cell engagers in cancer and infectious diseases. Cell. Mol. Immunol. *21*, 643–661. https://doi.org/10.1038/s41423-024-01176-4.
68. Fouts, A.E., Comps-Agrar, L., Stengel, K.F., Ellerman, D., Schoeffler, A.J., Warming, S., Eaton, D.L., and Feierbach, B. (2014). Mechanism for neutralizing activity by the anti-CMV gH/gL monoclonal antibody MSL-109. Proc. Natl. Acad. Sci. USA *111*, 8209–8214. https://doi.org/10.1073/pnas.1404653111.
69. Zheng, S.Q., Palovcak, E., Armache, J.P., Verba, K.A., Cheng, Y., and Agard, D.A. (2017). MotionCor2: anisotropic correction of beam-induced motion for improved cryo-electron microscopy. Nat. Methods *14*, 331–332. https://doi.org/10.1038/nmeth.4193.
70. Zhang, K. (2016). Gctf: Real-time CTF determination and correction. J. Struct. Biol. *193*, 1–12. https://doi.org/10.1016/j.jsb.2015.11.003.
71. Liebschner, D., Afonine, P.V., Baker, M.L., Bunkóczi, G., Chen, V.B., Croll, T. I., Hintze, B., Hung, L.W., Jain, S., McCoy, A.J., et al. (2019). Macromolecular structure determination using x-rays, neutrons and electrons: recent developments in phenix. Acta Crystallogr. D Struct. Biol. *75*, 861–877. https://doi.org/10.1107/S2059798319011471.
72. Pettersen, E.F., Goddard, T.D., Huang, C.C., Couch, G.S., Greenblatt, D. M., Meng, E.C., and Ferrin, T.E. (2004). UCSF Chimera–a visualization system for exploratory research and analysis. J. Comput. Chem. *25*, 1605–1612. https://doi.org/10.1002/jcc.20084.
73. Emsley, P., Lohkamp, B., Scott, W.G., and Cowtan, K. (2010). Features and development of Coot. Acta Crystallogr. D Biol. Crystallogr. *66*, 486–501. https://doi.org/10.1107/S0907444910007493.
74. Scheres, S.H.W. (2012). RELION: implementation of a Bayesian approach to cryo-EM structure determination. J. Struct. Biol. *180*, 519–530. https://doi.org/10.1016/j.jsb.2012.09.006.
75. Morris, L., Chen, X., Alam, M., Tomaras, G., Zhang, R., Marshall, D.J., Chen, B., Parks, R., Foulger, A., Jaeger, F., et al. (2011). Isolation of a human anti-HIV gp41 membrane proximal region neutralizing antibody by antigen-specific single B cell sorting. PLoS One *6*, e23532. https://doi.org/10.1371/journal.pone.0023532.
76. Wang, Y., Wu, C., Yu, J., Lin, S., Liu, T., Zan, L., Li, N., Hong, P., Wang, X., Jia, Z., et al. (2021). Structural basis of tetanus toxin neutralization by

native human monoclonal antibodies. Cell Rep. *35*, 109070. https://doi.org/10.1016/j.celrep.2021.109070.

77. Liao, H.X., Levesque, M.C., Nagel, A., Dixon, A., Zhang, R., Walter, E., Parks, R., Whitesides, J., Marshall, D.J., Hwang, K.K., et al. (2009). High-throughput isolation of immunoglobulin genes from single human B cells and expression as monoclonal antibodies. J. Virol. Methods *158*, 171–179. https://doi.org/10.1016/j.jviromet.2009.02.014.

78. Nicely, N.I., Dennison, S.M., Spicer, L., Scearce, R.M., Kelsoe, G., Ueda, Y., Chen, H., Liao, H.X., Alam, S.M., and Haynes, B.F. (2010). Crystal structure of a non-neutralizing antibody to the HIV-1 gp41 membrane-proximal external region. Nat. Struct. Mol. Biol. *17*, 1492–1494. https://doi.org/10.1038/nsmb.1944.

79. Pettersen, E.F., Goddard, T.D., Huang, C.C., Meng, E.C., Couch, G.S., Croll, T.I., Morris, J.H., and Ferrin, T.E. (2021). UCSF ChimeraX: Structure visualization for researchers, educators, and developers. Protein Sci. *30*, 70–82. https://doi.org/10.1002/pro.3943.

80. Case, D.A., Cheatham, T.E., Darden, T., Gohlke, H., Luo, R., Merz, K.M., Onufriev, A., Simmerling, C., Wang, B., and Woods, R.J. (2005). The Amber biomolecular simulation programs. J. Comput. Chem. *26*, 1668–1688. https://doi.org/10.1002/jcc.20290.

81. Maier, J.A., Martinez, C., Kasavajhala, K., Wickstrom, L., Hauser, K.E., and Simmerling, C. (2015). ff14SB Improving the Accuracy of Protein Side Chain and Backbone Parameters from ff99SB. J. Chem. Theor. Comput. *11*, 3696–3713. https://doi.org/10.1021/acs.jctc.5b00255.

82. Case D.A., Ben-Shalom I.Y., Brozell S.R., Cerutti D.S., Cheatham T.E., Cruzeiro V.W.D., Darden T.A., Duke R.E., Ghoreishi D., Gilson M.K., et al. (2018). AMBER 2018. https://doi.org/10.13140/RG.2.2.31525.68321.

83. Liu, X., Peng, L., and Zhang, J.Z.H. (2019). Accurate and Efficient Calculation of Protein-Protein Binding Free Energy-Interaction Entropy with Residue Type-Specific Dielectric Constants. J. Chem. Inf. Model. *59*, 272–281. https://doi.org/10.1021/acs.jcim.8b00248.

84. Wang, E., Weng, G., Sun, H., Du, H., Zhu, F., Chen, F., Wang, Z., and Hou, T. (2019). Assessing the performance of the MM/PBSA and MM/GBSA methods. 10. Impacts of enhanced sampling and variable dielectric model on protein-protein Interactions. Phys. Chem. Chem. Phys. *21*, 18958–18969. https://doi.org/10.1039/c9cp04096j.

85. Yang, Z., Li, G., Zhao, Y., Zhang, L., Yuan, X., Meng, L., Liu, H., Han, Y., Jia, L., and Zhang, S. (2021). Molecular Insights into the Recruiting Between UCP2 and DDX5/UBAP2L in the Metabolic Plasticity of Non-Small-Cell Lung Cancer. J. Chem. Inf. Model. *61*, 3978–3987. https://doi.org/10.1021/acs.jcim.1c00138.

## STAR★METHODS

### KEY RESOURCES TABLE

| REAGENT or RESOURCE | SOURCE | IDENTIFIER |
|---|---|---|
| Antibodies | | |
| PE-Cy5 Mouse Anti-Human CD16 | BD Biosciences | Cat# 555408; RRID: AB_395808 |
| PE Mouse Anti-Human IgD | BD Biosciences | Cat# 555779; RRID: AB_396114 |
| FITC Mouse Anti-Human CD14 | BD Biosciences | Cat# 555397; RRID: AB_395798 |
| PE-Cy5 Mouse Anti-Human CD3 | BD Biosciences | Cat# 555341; RRID: AB_395747 |
| APC-H7 Mouse Anti-Human CD19 | BD Biosciences | Cat# 560177; RRID: AB_1645470 |
| PE Mouse Anti-Human CD235a | BD Biosciences | Cat# 555570; RRID: AB_395949 |
| PE Goat Anti-Human IgG | Thermo Fisher Scientific | Cat# 12-4998-82; RRID: AB_465926 |
| PE Goat Anti-Rabbit IgG | Thermo Fisher Scientific | Cat# P-2771MP; RRID: AB_2539845 |
| Goat Anti-Human IgG HRP | Promega | Cat# W4031; RRID: AB_430835 |
| Goat Anti-Human IgG FITC | Solarbio | Cat# SF101 |
| Goat Anti-Mouse IgG FITC | Solarbio | Cat# SF131 |
| Goat Anti-Mouse IgG-HRP | Promega | Cat# W4021; RRID: AB_430834 |
| Goat Anti-Human IgG-HRP | Promega | Cat# W4301 |
| Rabbit Anti-Human CD64 | Abcam | Cat# ab196571 |
| PE Goat Anti-Rabbit IgG | SouthernBiotech | Cat# 4030-09; RRID: AB_2795937 |
| PE-Cy5 Mouse Anti-human IgG | BD Biosciences | Cat# 551497; RRID: AB_394220 |
| 8F9 | Thomson et al.[38] | mAb produced in this study |
| SM5-1 | Spindler et al.[35] | mAb produced in this study |
| 1G2 | Chandramouli et al.[36] | mAb produced in this study |
| SM10 | Pötzsch et al.[17] | mAb produced in this study |
| MSL-109 | Fouts et al.[68] | mAb produced in this study |
| Mouse Anti-CMV gH | Santa Cruz Biotechnology | Cat# sc-58113 |
| Mouse Anti-cytomegalovirus IE1 and IE2 | Abcam | Cat# ab53495; RRID: AB_882995 |
| Cells and virus strains | | |
| HEK293T/17 | ATCC | Cat# CRL-11268; RRID:CVCL_1926 |
| Expi293F Cells | Thermo Fisher Scientific | Cat# A14527 |
| HEK293S GnTI$^{-}$ Cells | Thermo Fisher Scientific | N/A |
| MRC-5 Cells | ATCC | Cat# CCL-171; RRID:CVCL_0440 |
| ARPE-19 | ATCC | Cat# CRL-2302; RRID:CVCL_0145 |
| CHO cells | Horizon Discovery | NA |
| gB-stabilized CHO cells | This paper | NA |
| HCMV Towne strain | Rutgers University, USA | N/A |
| HCMV TB40/E strain | Pasteur Institute, China | N/A |
| HCMV BE13/2012 strain | Anhui Medical University | N/A |
| VR1814 | Rutgers University, USA | N/A |
| NR | Rutgers University, USA | N/A |
| Chemicals and proteins | | |
| 0.25% Trypsin-EDTA(1X) | Gibco | Cat# 25200-072 |
| Dulbecco's Modified Eagle Medium | Gibco | Cat# C11885500BT |
| 2xDMEM | GENOM, China | Cat# GNM12902-2 |
| Fetal bovine serum (FBS) | Gibco | Cat# 16000-044 |
| Penicillin-streptomycin | Gibco | Cat# 15140-122 |
| FreeStyle™ 293 Expression Medium | Gibco | Cat# 12338-018 |
| PBS | Gibco | Cat# C10010500BT |

(*Continued on next page*)

*Continued*

| REAGENT or RESOURCE | SOURCE | IDENTIFIER |
|---|---|---|
| Dithiothreitol (DTT) | Sigma-Aldrich | Cat# D9779 |
| Iodoacetamide (IAM) | Sigma-Aldrich | Cat# I1149 |
| Trifluoroacetic acid (TFA) | Sigma-Aldrich | Cat# 91707 |
| NP-40 | Thermo Fisher Scientific | Cat# 85124 |
| Triton X-100 | Solarbio | Cat# T8200 |
| Tween 20 | Solarbio | Cat# T8220 |
| 4% Paraformaldehyde | Biosharp | Cat# BL539A |
| $MgCl_2$ | Sigma-Aldrich | Cat# M8266 |
| dNTPs | New England Biolabs | Cat# N0447 |
| HRP substrate (DAB) | MXB® Biotechnologies | Cat# DAB-0031 |
| Dimethy sulfoxide | Sigma-Aldrich | Cat# D2650 |
| BeyoECL Plus | Beyotime | Cat# P0018S |
| TMB Chromogen Solution | Solarbio | Cat# PR1200 |
| Normal Goat Serum | Solarbio | Cat# SL038 |
| HBS-EP+ buffer 10X | GE Healthcare | Cat# BR100669 |
| Glycine HCl (for antibody elution) | GE Healthcare | Cat# BR100354 |
| QuickAntibody-Mouse5W adjuvant | Beijing Biodragon, China | Cat# KX0210041 |
| $gB^{ECD}$ | This paper | NA |
| $gB^{ECD}$-698glyco | This paper | NA |
| AD-5 | This paper | NA |
| Streptavidin-BV421 | Biolegend | Cat# 405225 |
| Streptavidin-PE-Cy7 | BD Biosciences | Cat# 557598 |
| Hoechst 33342 | Solarbio | Cat# C0030 |
| DAPI | Sigma-Aldrich | Cat# D9542 |
| Evans Blue | Sigma-Aldrich | Cat# E2129 |
| Peroxidase Streptavidin | Abcam | Cat# ab7403 |
| (PE conjugated) HCV-E2 core | This paper | NA |
| (PE conjugated) RVG-hFc | This paper | NA |
| Human CD64, His Tag | ACRO Biosystems | Cat# FCA-H52H1 |
| Human CD32a(H131) | ACRO Biosystems | Cat# CD8-H5223 |
| Human CD16a(V158) | ACRO Biosystems | Cat# CD8-H52H4 |
| Complement factor C1q | Abcam | Cat# ab96363 |
| Low-Tox® Guinea Pig Complement | Cedarlane | Cat# CL4051 |
| SYBR Green I | Thermo Fisher Scientific | Cat# 4472918 |
| **Critical commercial assays** | | |
| Reverse transcriptase | Thermo Fisher Scientific | Cat# EP0442 |
| iProof High-Fidelity DNA Polymerase | BIO-RAD | Cat# 1725302 |
| Q5 Site-Directed Mutagenesis Kit | New England Biolabs | Cat# E0552S |
| Q5 High-Fidelity DNA Polymerase Mix | New England Biolabs | Cat# M0491 |
| Bio-Lite™ Luciferase Assay System | Vazyme | Cat# DD1201-02 |
| CellTiter-Glo Luminescent Cell Viability Assay | Promega | Cat# G7571 |
| EZ-Link™ Sulfo-NHS-Biotin | Thermo Fisher Scientific | Cat# 21217 |
| HiPure Plasmid EF Micro Kit | Magen | Cat# P1111 |
| NucleoBond Xtra Maxi Plus | MACHEREY-NAGEL | Cat# 740416 |
| Human Antibody Capture Kit | GE Healthcare | Cat# BR100839 |
| Anti-his Antibody Capture Kit | GE Healthcare | Cat# 28995056 |
| E.Z.N.A.Viral DNA Kit | OMEGA | Cat# D3396-01 |
| PNGase F | New England Biolabs | Cat# P0704L |
| Effectene® Transfection Reagent | QIAGEN | Cat# 301427 |

(*Continued on next page*)

*Continued*

| REAGENT or RESOURCE | SOURCE | IDENTIFIER |
|---|---|---|
| Recombinant DNA | | |
| $gB^{ECD}$ gene: (GenBank: FJ616285.1) | GenScript | N/A |
| C.$gB^{ECD}$ gene | GenScript | N/A |
| AD-5 gene: (GenBank: FJ616285.1) | GenScript | N/A |
| Full-length gB gene: (GenBank: FJ616285.1) | GenScript | N/A |
| pcDNA3.1(+) vector | Thermo Fisher Scientific | Cat# V79020 |
| Software and algorithms | | |
| FlowJo | BD biosciences | https://www.flowjo.com/ |
| IMGT/V QUEST | IMGT | https://www.imgt.org/IMGT_vquest/ |
| PRISM Graphpad | GraphPad software, LLC | https://www.graphpad.com/ |
| MotionCor2 | Zheng et al.[69] | https://msg.ucsf.edu/software |
| Gctf | Zhang et al.[70] | https://www.mrc-lmb.cam.ac.uk/kzhang/Gctf/ |
| PHENIX | Liebschner et al.[71] | https://www.phenix-online.org/ |
| UCSF Chimera | Pettersen et al.[72] | https://www.cgl.ucsf.edu/chimera/ |
| Coot | Emsley et al.[73] | https://www2.mrc-lmb.cam.ac.uk/personal/pemsley/coot/ |
| Pymol | Schrodinger, 2015 | https://pymol.org/2/ |
| RELION 3.1.1 | Scheres et al.[74] | https://www3.mrc-lmb.cam.ac.uk/relion/index.php/Main_Page |
| NUIFI software | Waters | N/A |
| Sequence LOGO Map | GENE DE NOVO | https://www.omicshare.com/tools/Home/Soft/seqlogo |
| Deposited data | | |
| Cryo-EM structure of HCMV glycoprotein B in complex with 1B03 Fab | This paper | PDB: 7YRN |
| HCMV glycoprotein B+1B03 Fab composite EM map | This paper | EMDB ID: 34063 |
| Others | | |
| Ficoll-Paque PLUS | GE Healthcare | Cat# 17-1440-02 |
| Superdex200 column | GE Healthcare | Cat# 28-9909 |
| 4-12% Bis-Tris SDS-PAGE gels | Invitrogen | Cat# NP0321BOX |
| Agarose | Baygene | Cat# BY-R0100 |
| iBlot Gel Transfer Stacks PVDF | Thermo Fisher Scientific | Cat# IB24001 |
| Ni-NTA Agarose | GE Healthcare | Cat# 17524801 |
| Protein A Resin | GenScript | Cat# L00210 |
| KappaSelect | GE Healthcare | Cat# 17-5458-01 |
| CM5 sensor chip | GE Healthcare | Cat# BR100012 |
| C1 sensor chip | GE Healthcare | Cat# BR100540 |

## EXPERIMENTAL MODEL AND STUDY PARTICIPANT DETAILS

### Human blood sample collection

Human blood samples from healthy adult individuals were collected with informed written consent following an IRB protocol approved by Medical Ethics Committee of the First Affiliated Hospital of Jinan University, Guangzhou, China.

### Cells and viruses

For recombinant protein expression, mammalian cells (Expi293F and HEK293S GnTI$^-$ Cells, Thermo Fisher) were cultured in suspension in GIBCO FreeStyle 293 Expression Medium (Thermo Fisher) for 5–7 days at 37°C, with 70% humidity and 8% $CO_2$ and rotating at 130 rpm/min. For neutralization assays, mammalian cells (ARPE-19 and MRC-5 cells, ATCC) were cultured in GIBCO DMEM

Medium (Thermo Fisher) at 37°C/5% $CO_2$ and passaged every 2 or 4 days. Laboratory Towne strain was kindly provided by Dr. Hua Zhu, Department of Microbiology, Biochemistry and Molecular Genetics, Rutgers University, USA. Clinical isolates VR1814 and NR were stored in Dr. Zhu's Lab. Laboratory TB40/E strain was kindly donated from Prof. Zhikang Qian, Pasteur Institute of Microbiology, Shanghai, China. Towne and TB40/E strains used in this study were fused to express GFP. BE13/2012 strain obtained from a clinical sample was kindly provided by Prof. Mingli Wang, Anhui Medical University, Hefei, Anhui Province, China.

### Mice

Four-week-old BALB/c mice (SPF) were purchased from Zhuhai BesTest Bio-Tech Co., Ltd, Guangdong, China. All mice were maintained in a specific pathogen-free vivarium, housed in temperature-controlled rooms, and had access to food and water *ad libitum*. Mice of five weeks old were used for studying immunogenicity. All animal experiments were conducted according to the guidelines of the Laboratory Animal Welfare Ethics Review and Use of Zhuhai BesTest Bio-Tech Co., Ltd, IAC(S)2001003-1.

## METHOD DETAILS

### hCMV antigens

The full-length gene sequences of hCMV gB from a total of 61 strains, including the Towne strain (accession no. FJ616285.1), were obtained from the NCBI GenBank. The consensus gB (C.gB) was derived from the conserved amino acid residues by aligning the gB sequences from the 61 hCMV strains. DNA constructs encoding the gB ectodomain (residues 1–698) of the Towne strain ($gB^{ECD}$), consensus ($C.gB^{ECD}$) and AD-5 (residues 134–343), fused to a 7-histidine tag at the C terminus, were designed and codon-optimized for expression in Expi293F cells (Thermo Fisher) with an optimal Kozak sequence (GCCACC). These constructs were *de novo* synthesized and subcloned into the eukaryotic expression vector pCDNA3.1$^+$ (Thermo Fisher) using the *Nhe*I and *Xba*I restriction sites. Mutations (Ile156His, His157Arg, Trp240Asn, Tyr242Thr, Cys246Ser, located in the fusion subdomain and 457-ETKE-460, substitution of the furin cleavage sites[34]) were introduced into $gB^{ECD}$ to generate $gB^{ECD}$-698glyco (residues 1–698) and its mutants using Q5 Site-Directed Mutagenesis Kit (New England Biolabs).[36] Stabilized prefusion gB was designed and expressed referred to the previous report.[37] All the proteins were produced in Expi293F cells, except for $gB^{ECD}$-698glyco, which was used for cryo-EM in HEK293S GnTI$^-$ cells (Thermo Fisher) and purified by Ni-NTA agarose (GE Healthcare). The purity and identity of the proteins were confirmed by 4–12% Bis-Tris SDS-PAGE gels (Thermo Fisher) and Western blots. The purified proteins were stored at −80°C before use in ELISA or SPR binding assays.

### Single B cell sorting and cloning of antibody variable genes

PBMCs were isolated from the peripheral blood of latently hCMV-infected individuals using Ficoll-Paque PLUS (GE Healthcare) density gradient centrifugation. Single memory B cells with antigen-specific B cell receptors (BCR) were sorted using fluorescence dye-labeled hCMV gB proteins as probes. Sorting was performed using fluorescence-activated cell sorting (FACS) on the BD FACS Aria III platform as previously described,[75,76] based on set sorting logic gates (CD3-/CD14-CD16-/CD235a-/CD19+/SIgD-/labeled $gB^{ECD}$+ and $C.gB^{ECD}$+) (BD Biosciences and Thermo Fisher). The data were analyzed using FlowJo software (https://www.flowjo.com/). To increase sorting specificity, two fluorescein reagents (Phycoerythrin-canin7, PE-Cy7 and Brilliant Violet, BV421) (BD Biosciences and Biolegend) were used to label $gB^{ECD}$ and $C.gB^{ECD}$. The variable region gene segments Ig heavy- and light-chain ($V_HDJ_H$ and $V_LJ_L$) were amplified from sorted single B cells by reverse transcription and nested PCR, as previously reported.[77] Functional $V_HDJ_H$ and $V_LJ_L$ genes were sequenced, annotated using IMGT/V-QUEST (https://www.imgt.org/IMGT_vquest/), and assembled into full-length Ig heavy- and light-chain linear expression cassettes using one-step overlapping PCR.[77]

### Expression and purification of recombinant IgG and Fab

The $V_HDJ_H$ and $V_LJ_L$ genes from 42 gB-reactive mAbs were selected to subclone into the pCDNA3.1$^+$ mammalian expression vector, which contains the human IgG1 heavy-chain constant region gene, kappa or lambda light chain constant region gene. This allowed for the production of full-length antibodies through transient transfection.[77] The recombinant 1B03 Fab was produced through transient transfection using constructs of human Fab heavy-chain and kappa light chain genes, as described in a previous study.[78] Both the recombinant IgG and IB03 Fab were produced in Expi293F cells and purified using Protein A column chromatography (GenScript) for full-length IgG and KappaSelect column chromatography (GE Healthcare) for IB03 Fab.[78] Reference nAbs (8F9, SM5-1, 1G2, and MSL-109) were produced recombinantly based on the sequences deposited in PDB database.

### Virus neutralization assays

Neutralization activity of mAbs against laboratory strains of Towne and TB40E were evaluated in MRC-5 cells (ATCC). MRC-5 cells were seeded at a density of 1 × 104 per well in black 96-well plates with transparent bottom (Costar, USA). The laboratory strain Towne or TB40/E (MOI = 1) was preincubated with eight 3-fold serial dilutions of mAbs in a volume of 50 μL in Dulbecco's Modified Eagle Medium (DMEM, Gibco) for 1 h at 37°C. The mixtures were added to MRC-5 cells and incubated for 4 h at 37°C, followed by the addition of 100 μL of DMEM containing 2% fetal bovine serum (FBS, Gibco). The cells were cultured at 37°C/5% $CO_2$ for 96 h. The intracellular fluorescence intensity of GFP in the infected cells was measured by SpectraMax Paradigm (Molecular Devices) after fixation with 4% paraformaldehyde (Biosharp). The antiviral activity of the antibodies was evaluated by their relative fluorescence

intensity. A similar neutralization method was applied to assess the neutralization activity of human and mouse immune sera against the Towne strain.

Neutralization assays for clinical isolates VR1814 and NR (MOI = 0.01, about 400 plaque-forming units, PFU) were assessed in ARPE-19 cells (ATCC) by the reduction of the fluorescent cell counts. The infected monolayer cells were cultured for 20–28 h at 37°C/5% $CO_2$, fixed with 4% paraformaldehyde for 25 min, permeabilized with 0.5% Triton X-100 (Solarbio) for 10 min, washed three times with wash buffer (PBS/0.1% Tween 20, PBST), and blocked with PBST/5% goat serum for 1 h at room temperature (RT). The plates were then incubated for 2 h at RT with mouse anti-hCMV IE1/IE2 antibody (Abcam, 1:500). After washing the plates three times, they were incubated for another hour at RT with goat anti-mouse IgG (FITC) (Solarbio, 1:500) and then washed three times with PBST. Counting fields were captured using an EVOS FL AUTO2 microscope (Thermo Fisher), and numbers of infected cells reflected as fluorescence-positive cells were counted to calculate the $EC_{50}$ of the tested antibodies by nonlinear regression fit. $EC_{50}$ was defined as yielding a 50% reduction in fluorescent-positive cells in comparison with the numbers of the virus control. Neutralization activity against clinical isolate BE13/2012 by antibodies were assessed by the reduction of virus-specific cytopathic plaque counts after cultured for 96 h at 37°C/5% $CO_2$.

### ELISA assays for cross-competitive binding

The biotin labeling of individual antibodies was performed using the EZ-Link Sulfo-NHS-Biotin kit (Thermo Fisher). Sub-saturating concentrations of the biotinylated antibodies were determined by measuring the $OD_{450}$ absorbance value close to saturation. Briefly, 96-well high-binding ELISA plates (Thermo Fisher) were coated with gB antigen (50 ng/well) in carbonate buffer ($Na_2CO_3$/$NaHCO_3$, pH 8.0) overnight at 4°C, then blocked with PBS containing 0.05% Tween 20 and 5% w/v goat serum (Solarbio) for 2 h at RT. Serial dilutions of unlabeled competitive antibodies (aliquots 50 μL of 5-fold serial dilutions, originating from 1 μg/mL) were mixed with sub-saturating concentrations of biotin-labeled antibodies (50 μL). The mixtures were then added to the coated plates, and incubated for 1 h at 37°C. The plates were washed three times with PBST and incubated with streptavidin HRP (Abcam, 1:10000) at 37°C for 1 h, washed five times and then developed with 100 μL/well TMB substrate (Solarbio). The chromogenic reaction was stopped with addition of 50 μL/well 2 M $H_2SO_4$ and detected at $OD_{450}$ using a SpectraMax Paradigm. The competition ratio was calculated as follows: $OD_{450(\text{lowest competitive antibody})}$-$OD_{450(\text{highest competitive antibody})}$/$OD_{450(\text{lowest competitive antibody})}$.

### Immunoprecipitation of hCMV virion with antibodies

Aliquots of 100 μg of individual antibodies were incubated with Protein A-agarose resins (Thermo Fisher) at 4°C overnight. HCMV virion preparation at $1 \times 10^6$ PFU was added to tubes containing individual antibodies captured by Protein A and incubated at 4°C for 1 h in a final volume of 5 mL. The antibody-virion-Protein A complexes were washed three times with 10 mL of protein A binding buffer, eluted with 5 mL of IgG elution buffer, and then concentrated to a final volume of 100 μL for each sample. The immunoprecipitated samples in denaturing buffer were boiled for 10 min, fractionated on 4–12% SDS-PAGE (Thermo Fisher), and then either stained with Coomassie blue or immunoblotted with hCMV-positive serum and anti-gH antibody (Santa Cruz Biotechnology) to detect virus-associated proteins.

### Virus adsorption and effect of antibodies on virus entry

Aliquots of MRC-5 cells at $2\times10^4$ per well in a volume of 150 μL were seeded in 96-well plates. Aliquots of Towne strain stock (MOI = 1) were preincubated with individual mAbs at a concentration of 10 μg/mL at 37°C for 1 h. The virus/mAbs mixtures and the cells were separately precooled to 4°C for 15 min before the mixtures were added to the cells. Heparin known to block CMV adsorption to cells was used as a positive control. Following incubation at 4°C for 1 h, the cells were washed three times with ice-cold PBS and lysed with lysis buffer (Thermo Fisher) for 2–5 min. Total DNAs were extracted from cell lysates using E.Z.N.A.Viral DNA Kit (Omega). The relative copy numbers of HCMV-specific gene *UL75* were determined by quantitative real-time PCR (Bio-Rad) stained with SYBR Green I (Thermo Fisher) in parallel to *GAPDH* as an internal reference. Primers: *qGAPDH*_F AGAAGGCTGGGGCTCATTTG; *qGAPDH*_R AGGGGCCATCCACAGTCTTC; *qUL75*_F:GGTTTCTAGCGTGCTTGGTTGCATG; *qUL75*_R:CAGCGACCTGTACACAC CCTGTTCC. In virus entry assays, the precooled cells seeded in black 96-well plates with transparent bottom were preincubated with Towne strain (MOI = 1) at 4°C for 1 h, washed with ice-cold PBS and incubated at 37°C for 96 h with three 10-fold serial dilutions of mAbs. Subsequent steps were similar to the procedure for virus neutralization assays described above.

### Inhibition assays for cell-to-cell spread of hCMV

MRC-5 cells at $8\times10^4$ per well grown in 96-well plates were infected with 50 μL of diluted virus stock (MOI = 0.0025, approximately 200 PFU of Towne strain). Four hours after infection, virus inoculum was removed and replaced with an agarose overlay medium. The overlay medium was prepared as follows: 0.8% agarose (Baygene) was mixed 1:1 with 2x DMEM (GENOM, China) supplemented with 20% FBS, 2% penicillin-streptomycin (Gibco), and containing the respective antibodies (50 μg/mL or dilutions thereof) at 45°C in a water bath. Cells were cultured at 37°C/5% $CO_2$ for 5 days. Follow-up steps referred to the neutralization assays for clinical isolates VR1814 and NR. The difference was that the secondary antibody incubated was goat anti-mouse IgG HRP (Promega, 1:2000), while the DAB (MXB Biotechnologies, 1:20) was used as its chromogenic agent. The chromogenic reaction was maintained

under light-proof condition for 2–5 min, then used deionized water to end the reaction. Images were captured using an EVOS FL AUTO2 microscope. The inhibitory efficacy of other cluster I nAbs at a given concentration (25 μg/mL) on viral cell-to-cell spread was evaluated in the same way.

### Antibody-mediated ADCC, ADCP and CDC assays

ADCC and ADCP assays: Antibodies with a starting concentration of 24 μg/mL in CD Forti CHO Medium (Thermo Fisher) were diluted 5-fold for 8 gradients. Aliquots of 25 μL/well of the diluted antibody solution were added to an opaque white 96-well cell culture plate (Costar, USA) containing target cells (gB-stabilized CHO cells, $1\times10^6$/mL, 25 μL/well) and incubated at 37°C for 30 min. Then the effector cells (Jurkat-FcγRIIIa V158 or Jurkat-FcγRIIa H131 cells, $6\times10^6$/mL, 25 μL/well) (Vazyme) were added and co-cultured at 37°C/5% $CO_2$ for 6 h, followed by equilibration at RT for 5 min. Aliquots of 75 μL/well of the Luciferase substrate solution (Vazyme) were added to the plates and incubated at RT for 5 min. The plates were detected with Microplate Reader (BioTek). CDC assays: Antibodies were diluted 3-fold for 9 gradients from a starting concentration at 80 μg/mL in CD Forti CHO Medium. Aliquots of 50 μL/well of the diluted antibody solution were added to an opaque white 96-well cell culture plates containing target cells (gB-stabilized CHO cells, $6\times10^5$/mL, 50 μL/well) and incubated at 37°C for 30 min. Aliquots of 5 μL/well of the guinea pig serum were added and co-cultured at 37°C/5% $CO_2$ for 5 h, followed by equilibration at RT for 5 min. Aliquots of 100 μL/well of the CellTiter-Glo solution (Promega) were added to the plates and incubated at RT for 5 min. The plates were detected with Microplate Reader (BioTek).

### Detection of antibodies entered the cells by immunofluorescence

MRC-5 cells at $2\times10^3$ per laser confocal dish grown for 24 h were infected with Towne strain (MOI = 0.5) for 4 h, then washed the cells with PBST and added 1 mL of fresh medium containing 10 μg/mL of antibody (3B06, 1B03 and MSL-109) or protein (HCV-E2 and RVG-hFc). The cells were washed three times with PBST after incubation for 2 days, then added 4% paraformaldehyde to fix the cells for 10–15 min, and treated the cells with 0.5% Triton X-100 permeabilized for 5–10 min. Incubated cells with 5% goat serum at 37°C for 1 h, then added PE-Cy5 mouse anti-human IgG diluted (1:1000) with 5% goat serum at 37°C for 1 h. Washed the cells with PBST for three times and added 10 μg/mL Hoechst for 5 min. The laser confocal microscopy (OLYMPUS2) was used to detect the fluorescent signals of individual channels.

### Passages of hCMV virus with antibody

Aliquots of MRC-5 cells at $1\times10^5$ per well in a volume of 2 mL were seeded in 6-well plates. Aliquots of Towne strain stock (MOI = 0.1) were added and incubated for 4 h. Then, virus inoculum was removed from plates followed by washing twice with PBS. After washing, the infected cultures were fed with 2 mL/well of fresh DMEM medium containing either 100 μg/mL of mAb MSL-109 or 10 μg/mL of mAb 1B03. Virus infection was evaluated by fluorescence microscopy after incubation at 37°C/5% $CO_2$ for 3 days. After removing the culture medium followed by washing three times with PBS, the infected cells were collected from the plates with 2 mL antibody-free fresh medium. The cells suspensions were fast frozen and thawed three times. The infected cell supernatants were collected by centrifugation at 4000*g*/min at 4°C for 1 h. Aliquots of 0.25 mL of the infected cell supernatants were used for the next round of virus infection, then supplemented with fresh medium containing either 100 μg/mL of mAb MSL-109 or 10 μg/mL of mAb 1B03 after infection for 4 h. This procedure was used for a total of three rounds of virus passaging.

### Characterization of the molecular basis of antibody biological functions

Binding of 1B03/$gB^{ECD}$ complex to FcγRII/III and complement factor C1q. The CM5 chip (GE Healthcare) was immobilized with anti-Histidine antibody to capture histidine-tagged FcγRIIa (CD32a) H131 or FcγRIIIa (CD16a) V158 proteins (ACRO Biosystems) at 200 RUs. Seven 2-fold serial dilutions of 1B03/$gB^{ECD}$ complex (starting at 12500 nM or 1000 nM) were injected at a rate of 25 μL/min for 90 s with a 300 s dissociation. For C1q binding, 1B03/$gB^{ECD}$ complex was captured using the Human Antibody Capture Kit, followed by injection of seven 2-fold serial dilutions of C1q protein (starting at 16 nM) at a rate of 25 μL/min for 90 s, with a 300 s dissociation.

Flow cytometric analysis of stably transfected gB expression CHO cells (gB.CHO). Surface expression of the stably transfected gB.CHO was validated by incubating CHO cells with 5 μg/mL of nAb 1B03 prepared in 2% FBS for 1 h at 4°C, followed by addition of PE-labeled goat anti-human IgG at a volume of 1:200 for 1 h at 4°C. The positivity rate of CHO cells overexpressing hCMV gB protein reached 87.5% (blue peak), and the mean fluorescence intensity increased approximately 5- to 10-fold compared to the negative control (red dashed peak). Immunofluorescence assays were performed by incubating CHO cells air-dried and fixed on slides with 10 μg/mL of nAb 1B03 prepared in 2% FBS for 1 h at 37°C, followed by addition FITC-labeled goat anti-human IgG diluted 1:200 for 1 h at 37°C. Nuclei were visualized using Evans Blue solution at a 1:100 dilution.

Detection of autoreactivity of nAb 1B03 with HEP-2 epithelial cells. HEP-2 cells were fixed with 4% paraformaldehyde for 10 min and permeabilized with 0.5% Triton X-100 for 10 min. Incubation with 50 μg/mL nAbs 1B03, anti-complement factor antibody (αCFH, known HEP-2 cells reactive mAb) and anti-respiratory syncytial virus antibody (αRSV, as a negative control) was carried out at RT for 2 h. Goat anti-human IgG/FITC was used at a 1:200 dilution in PBS for at RT 45 min, for detection of binding by the tested mAbs.

Detection of FcγRI(CD64) on MRC-5 cells induced by hCMV. MRC-5 cells infected with Towne (MOI = 0.1, fused to express GFP) were fixed and stained after 3 days of incubation. Green fluorescence indicated viral infection, while FcγRI (red) was detected using a rabbit anti-human CD64 (Abcam, 1:100) as the first antibody and a PE-conjugated goat anti-rabbit IgG (SouthernBiotech, 1:500) as the secondary antibody. Strong binding of nAb 1B03 (IgG1 subtype) to recombinant FcγRI(CD64) was observed using SPR. The CM5

chip (GE Healthcare) was immobilized with anti-histidine antibody to capture histidine-tag FcγRI(CD64) proteins (ACRO Biosystems) at 200 RUs. Seven 2-fold serial dilutions of nAb 1B03 (starting at 120 nM) were injected at a rate of 25 μL/min for 90 s, with a 300 s dissociation.

### Biochemical and FSEC analysis

Purified gB$^{ECD}$-698glyco and 1B03 Fab were analyzed via SDS-polyacrylamide gel electrophoresis (12%) in the presence of 0.5 M Dithiothreitol (DTT, Sigma-Aldrich). Protein bands were visualized by colloidal Coomassie blue staining. Fluorescence-detection size exclusion chromatography (FSEC) was conducted to verify the protein profile and trimeric assembly through using a Superose 6 Increase 10/300 GL column performed on a Shimadz FPLC-system (flowrate of 0.5 mL/min) in the TBS buffer containing 20 mM Tris-HCl pH 8.0, 150 mM NaCl. Individual 1B03 Fab, gB$^{ECD}$-698glyco or gB$^{ECD}$-698glyco/1B03 Fab complex (at 1:3 M ratio) were loaded.

### Cryo-EM sample preparation

Purified 1B03 Fab was incubated with gB$^{ECD}$-698glyco at a 3:1 M ratio per protomer for 10 min then ultracentrifuged 40,000 g at 4°C for 40 min. Size-exclusion chromatography was performed with a Superose 6 Increase 10/300 GL column on a Biorad NGC-system (flowrate of 0.5 mL/min) in TBS (20 mM Tris-HCl pH 8.0, 150 mM NaCl). The peak fraction corresponding to the gB$^{ECD}$-698glyco/1B03 Fab complexes were diluted to 0.175 mg/mL with TBS buffer and ultracentrifuged at 40,000 g, 4°C for 40 min 3 μL sample was applied to glow discharged Quantifoil grid 1.2/1.3 Au 300 mesh grids, and then blotted for 3s and plunge-frozen in liquid ethane using FEI Vitrobot with 100% humidity at 8°C.

### Cryo-EM data collection and processing

The grids were initially screened by FEI Talos 120KV microscope and then collected on a 300kV Titan Krios cryo electron microscope using EPU. Movies were collected using a Gatan K3 Summit direct electron detector in super-resolution mode at 81,000× magnification (unbinned pixel size of 0.428 Å/pixel) using a defocus range of −1 to −2.5 μm. All micrographs were collected with a total dose of ∼60 $e^{-}$/Å$^2$ over 40 frames.

Raw dataset was collected using super-resolution mode, 2x2 Fourier space binned raw data stack was motion corrected and dose weighted by MotionCor2 (https://msg.ucsf.edu/software).[69] Accurate estimation of contrast transfer function was estimated by Gctf (https://www.mrc-lmb.cam.ac.uk/kzhang/Gctf/).[70] About 80 micrographs were initially picked out for the reference-free particle picking using Laplacian-of-Gaussian based autopicking in Relion 3.1.1 (https://www3.mrc-lmb.cam.ac.uk/relion/index.php/Main_Page).[74]

Approximately 7000 particles were chosen for reference-free 2D classification. The selected 2D class averages were used as a template for autopicking in Relion. The particles were then taken for multi-round of 2D classification in Relion 3.1.1. The initial model was *de novo* generated in Relion. Followed 3D classification was with C1 symmetry to avoid reconstruction bias. After multi-round of 3D classification, 3D classes were inspected using UCSF Chimera (https://www.cgl.ucsf.edu/chimera/) and particles with clear fab binding were further selected for 3D refinement with C3 symmetry. CTF refinement and Bayesian polishing were applied to the reconstructed 3D classes and followed by another round of 3D refinement. All maps were postprocessed using a solvent mask with B-factors automatically estimated. Resolutions were estimated with the gold-standard Fourier shell correlation criterion of 0.143. Local resolution estimation was conducted in Relion 3.1.1.

### Atomic model building and refinement

The model of gB$^{ECD}$-698glyco was *de novo* generated by uni-Fold via Hermite platform, and the initial structure of 1B03 Fab was predicted using its antibody specialized version and docked into the cryo-EM density maps using UCSF Chimera.[72] Missing loops were manually built using Coot (https://www2.mrc-lmb.cam.ac.uk/personal/pemsley/coot/).[73] For areas with poorly resolved density, the residues were replaced by alanine. All structure refinements were carried out by real-space refinement in Phenix (https://www.phenix-online.org/)[71] with secondary structure and geometry restraints.

Modeled structures were generated by Pymol (https://pymol.org/2/), Chimera 1.6[72] and ChimeraX 1.3.[79] Specify for the structural analysis, center-of-mass (COM) was generated by Center-of-mass scripts in Pymol. The angles between space vectors connecting the COMs of gB/1B03 Fab (PDB: 7YRN) and gB/1G2 Fab (PDB: 5C6T,[36]) interface was calculated by formula below:

$$\theta = arccos\left(\frac{x_1x_2+y_1y_2+z_1z_2}{\sqrt{x_1^2+y_1^2+z_1^2}*\sqrt{x_2^2+y_2^2+z_2^2}}\right)$$

### Model construction of antigen-antibody interaction

The initial model of gB-AD-5 in complex with nAb 1B03 was built from the Cryo-EM structure of gB/1B03 complex. In accord to the amino acid sequence differences, the coordinates of gB-AD-5 region with identified neutralizing epitopes of 1B04, 1C03, 1C04, 1G03 and 3B01 were constructed by the MODELER program,[43] with the template of gB-AD-5/1B03 model. The generated six models were geometry-optimized using the conjugate gradient (CG) method, and further refined by the 100 ns explicit solvent molecular dynamics (MD) simulations. Each system was performed using AMBER18 software,[80] and the antigen and antibody were described using AMBER ff14SB force field.[81] The binding free energies ($\Delta G_{bind}$) were evaluated by the molecular mechanics generalized Born surface

area (MM/GBSA) approach in AmberTools18,[82] which has been successfully used to predict the binding affinities for a variety of protein-protein interactions.[83] The exterior (solvent) and interior dielectric constants were set to 80.0 and 1.0, respectively.[84] Details of the simulation were published previously,[85] and structural plotting and visualization were accomplished by Discovery studio client (Accelrys Inc.) and UCSF Chimera.[72]

### Binding affinity of antibody to hCMV gB or mutants by SPR

The affinity constants (*KD*) of 1B03 to $gB^{ECD}$-698glyco or mutants were determined by SPR using a Biacore 8K System (GE Healthcare). Anti-human IgG Fc antibody was covalently immobilized on the CM5 chip (GE Healthcare) to approximately 6000 response units (RUs) in two fluid channels by using a human antibody capture kit (GE Healthcare). MAb 1B03 was captured on Channel 2 to approximately 200 RUs, then five 2-fold serial dilutions of either $gB^{ECD}$-698glyco (starting at 48 nM), mutants (starting at 200 nM), $gB^{ECD}$-698glyco (starting at 20 nM) or deglycosylated $gB^{ECD}$-698glyco (starting at 50 nM) were injected at a rate of 30 μL/min for 90 s with a 600 s dissociation. Regeneration of the chip was achieved by injecting 3 M $MgCl_2$ for 30 s. Channel 1 of the chip served as a reference. All experiments were performed at RT and data were analyzed with Biacore 8K Evaluation Software (version: 2.0.1). The response units (RUs) of the whole process of association and disassociation for serial diluted analytes were fitted to the curves to obtain the association constant (*Ka*) and disassociation constant (*Kd*). *KD* was defined as the ratio of *Kd* to *Ka*.

### Epitope cross-competitive assay by SPR

Epitope competition assays of nAbs 1B03 and 1G2 (Figure 5C) were carried out in the competition module of the Biacore X100 system (GE Healthcare). Anti-his antibody was covalently immobilized on the C1 chip (GE Healthcare) to approximately 10000 RUs in two fluid channels by using His capture kit (GE Healthcare). His-tagged $gB^{ECD}$-698glyco was injected continuously at 400 μg/mL for 300 s to achieve approximately 600 RUs. MAb 1G2 was pre-sampled at 50 μg/mL for 60 s to achieve a stable value of 300 RUs of binding to $gB^{ECD}$-698glyco. MAb 1B03 was injected at 50 μg/mL for 60 s to detect the binding to gB proteins. After each cycle completed, glycine buffer (pH = 1.5) was used for regeneration of the chip.

### Structural analysis of N-glycosylation of hCMV gB AD-5

After reduction by DTT and alkylation by Iodoacetamide (IAM, Sigma-Aldrich) sequentially, aliquots of 200 μg of AD-5 protein in guanidine hydrochloride buffer (Sigma-Aldrich) were replaced with 8 M urea solution (Sigma-Aldrich). Aliquots of 40 μg of AD-5 protein in the urea solution were digested with trypsin (Gibco) for 4 h. Half of the samples were deglycosylated overnight with PNGase F (New England Biolabs). The remaining half of the samples were continued to be digested overnight with trypsin. Next, 20% Trifluoroacetic acid (TFA, Sigma-Aldrich) was added to terminate the reaction. Data were collected using ultra-performance liquid chromatography (UPLC I-Class/Xevo G2-XS, Waters)-Q-TOF mass spectrometry and analyzed with NUIFI software (Waters).

### Deglycosylation of gB

PNGase F can effectively cleave glycans when an α1-6 fucose is on the core GlcNAc. To observe the effect of deglycosylation of gB protein on the binding by mAb 1B03, $gB^{ECD}$ protein was either partially deglycosylated with increasing amounts of PNGase F (from 5 U to 500 U per μg of $gB^{ECD}$) under native condition for 24 h at 37°C, or completely deglycosylated with the excess amounts of PNGase F (500 U per μg of $gB^{ECD}$) for 24 h at 37°C after protein denaturation.

### Human serum neutralization assays

A total of 287 human serum samples were tested for neutralization activity. All serum samples were complement-inactivated and diluted at a working concentration of 1:50 against Towne strain (MOI = 1) in MRC-5 cells. The details of operation and detection methods refer to the section of virus neutralization assays in Methods. Human serum sample Ep0082 as a representative with high AD-5-reactive antibody titers, was selected for depletion of AD-5 reactivity by incubation with recombinant soluble AD-5 (50 μg/mL) for 1 h at RT. The AD-5-depleted and non-depleted serum with 3-fold serial dilutions starting from 1:10 were evaluated for neutralizing activity against Towne strain (MOI = 1) in MRC-5 cells.

### Mouse immunization and serum neutralization

All animal experiments were conducted according to the guidelines of the Laboratory Animal Welfare Ethics Review and Use of Zhuhai BesTest Bio-Tech Co., Ltd, IAC(S)2001003-1. Ten mice per group were immunized with either AD-5 or $gB^{ECD}$. Mice were immunized by an intramuscular injection with 20 μg of protein adjuvanted with water-soluble QuickAntibody-Mouse5W (Biodragon) in a volume of 100 μL for four times at 3-week intervals. Serum samples were collected before and two weeks after each immunization and heat-inactivated for 30 min at 56°C prior to use. Four 3-fold serial dilutions starting from 1:30 dilution of post-immune mouse sera was evaluated for neutralization activity against Towne strain (MOI = 1) and BE13/2012 in MRC-5 cells.

## QUANTIFICATION AND STATISTICAL ANALYSIS

Prism 8.0 software (GraphPad) was used for graphic plotting and statistical analysis. *p* values are considered statistically significant if $p < 0.05$. The error bars in the Figs represent the standard error of the mean (SEM.) or the standard deviation (SD.).